remote sensing

MDPI

Article

Exploring Topological Information Beyond Persistent Homology to Detect Geospatial Objects

Meirman Syzdykbayev [1,*] and Hassan A. Karimi [2]

[1] Department of Information Systems, SDU University, Kaskelen 040900, Kazakhstan
[2] School of Computing and Information, University of Pittsburgh, Pittsburgh, PA 15213, USA; hkarimi@pitt.edu
* Correspondence: meirman.syzdykbayev@sdu.edu.kz

Abstract: Accurate detection of geospatial objects, particularly landslides, is a critical challenge in geospatial data analysis due to the complex nature of the data and the significant consequences of these events. This paper introduces an innovative topological knowledge-based (Topological KB) method that leverages the integration of topological, geometrical, and contextual information to enhance the precision of landslide detection. Topology, a fundamental branch of mathematics, explores the properties of space that are preserved under continuous transformations and focuses on the qualitative aspects of space, studying features like connectivity and exitance of loops/holes. We employed persistent homology (PH) to derive candidate polygons and applied three distinct strategies for landslide detection: without any filters, with geometrical and contextual filters, and a combination of topological with geometrical and contextual filters. Our method was rigorously tested across five different study areas. The experimental results revealed that geometrical and contextual filters significantly improved detection accuracy, with the highest F1 scores achieved when employing these filters on candidate polygons derived from PH. Contrary to our initial hypothesis, the addition of topological information to the detection process did not yield a notable increase in accuracy, suggesting that the initial topological features extracted through PH suffices for accurate landslide characterization. This study advances the field of geospatial object detection by demonstrating the effectiveness of combining geometrical and contextual information and provides a robust framework for accurately mapping landslide susceptibility.

Keywords: persistent homology; TDA; LiDAR; landslide; object detection

check for updates

Citation: Syzdykbayev, M.; Karimi, H.A. Exploring Topological Information Beyond Persistent Homology to Detect Geospatial Objects. *Remote Sens.* **2024**, *16*, 3989. https://doi.org/10.3390/rs16213989

Academic Editor: Prasad S. Thenkabail

Received: 4 August 2024
Revised: 13 October 2024
Accepted: 21 October 2024
Published: 27 October 2024

Copyright: © 2024 by the authors. Licensee MDPI, Basel, Switzerland. This article is an open access article distributed under the terms and conditions of the Creative Commons Attribution (CC BY) license (https://creativecommons.org/licenses/by/4.0/).

1. Introduction

The term "geospatial object" encompasses various landscape elements, including water bodies, landslides, forests, and grasslands. These objects are characterized by indistinct boundaries and form part of the ambient environment, referring to geospatial entities situated in adjacent areas but not classified under the target object category [1]. Traditional methods for detecting geospatial objects face multiple challenges. Issues such as scalability arise from the significant variation in the size and shape of these objects. Additionally, occlusion, background clutter, and variations in illumination and shadow complicate the detection process due to the nature of data collection [2–4]. The detection of geospatial objects is a cornerstone of geospatial data analysis and is pivotal across a wide range of applications, including monitoring natural hazards, agriculture, and urban planning. Its fundamental goal is to identify and locate target objects within a geospatial dataset and determine their precise positions on the Earth's surface [5].

Topological data analysis (TDA) stems from extensive research in computational topology and data analytics [6] where it perceives a dataset as a set of points and aims to elucidate its structure, providing crucial insights into the dataset's shape, or in other words, its topological information. This includes information about the shape of the target geospatial object. Unlike the specific and fixed details provided by geometric information,

topological data offer a broad overview of the entire dataset across various scales [7]. TDA incorporates various tools, with persistent homology (PH) being the most prominent [6]. PH is designed to extract topological information from data by examining the corresponding data connections and gaps, enabling it to describe complex structures of a dataset, like loops and voids, which are often invisible with geometry-based methods [8].

Recent applications of PH in geospatial analysis have shown promising results. For instance, ref. [9] PH has been utilized to identify patterns in climate data, and ref. [10,11] has been applied to urban road network analysis, revealing underlying structural properties. In remote sensing, PH has been employed to enhance land cover classification [12]. These studies demonstrate the versatility of PH in handling complex spatial data and its potential to address challenges in geospatial object detection.

Traditional geospatial object detection methods have primarily relied on leveraging spectral, textural, morphological, geometrical, and contextual features extracted from remote sensing imagery [13,14]. These methods are often rooted in knowledge-based detection approaches, interpreting detection as a hypothesis testing problem that utilizes sets of knowledge and rules pertaining to these features [1]. While they have achieved success in various applications, they face limitations when dealing with objects exhibiting complex shapes, varying sizes, or subtle topographic features such as landslides [15]. Moreover, machine learning approaches like convolutional neural networks (CNNs) require large amounts of labeled data and may not generalize well across different geographical regions or sensor types [16]. Despite the comprehensive nature of these methods, they often fall short in fully exploiting the rich layer of topological information intrinsic to geospatial datasets. These shortcomings highlight the need for alternative approaches that can capture the inherent topological properties of geospatial objects.

This paper focused on the detection of landslides as target geospatial objects. There are numerous geospatial objects with distinct circular structures, such as craters or hurricanes. However, the choice of landslides as the focal geospatial object is guided by several compelling reasons:

- Landslides are among the most destructive natural hazards, representing potentially devastating geological events that not only claim lives but also lead to significant economic losses and adverse environmental impacts. According to the United Nations Office for Disaster Risk Reduction (UNDRR), landslides result in billions of dollars in damages globally each year [17]. These substantial impacts underscore the critical need for effective landslide detection and monitoring methods to mitigate risks and implement timely interventions. Landslide susceptibility maps, which include boundaries of existing landslides, serve as valuable tools to mitigate the loss of life and property associated with landslides.
- Delineation of existing landslide boundaries, typically achieved manually via remote sensing datasets like satellite imagery or Light Detection and Ranging (LiDAR) data, is a laborious and time-consuming process. This underscores the urgency for an automated or semi-automated landslide detection method [18,19].
- Landslides imprint unmistakable signs on the landscape, including alterations to slope shape, position, and surface appearance [20]. These alterations result in complex morphological characteristics—irregular shapes, varying sizes, and intricate boundary patterns—that pose significant challenges for traditional detection methods relying primarily on pixel intensity or spectral information. The aggregate view of linear topographic features, which can originate at the top, bottom, left, or right side of a landslide and form its boundaries, often exhibits a circular structure. PH offers a novel approach by focusing on the shape and connectivity of data. By analyzing the topological features of a dataset across multiple scales, PH captures essential geometric and topological information such as connected components, holes, and voids that persist over different spatial resolutions. Integrating PH into landslide detection allows for the effective identification and characterization of the complex shapes of landslides, leading to enhanced detection accuracy and a more robust identification process.

Advancements in technology and methodology have significantly transformed the landscape of landslide detection over the past decade. The transition from manual processes to the utilization of machine learning (ML), including deep learning (DL), represents a paradigm shift towards automating detection with unprecedented accuracy and efficiency. This evolution has been fueled by the increased availability of high-resolution satellites and airborne imagery, facilitating the identification of landslides [18,21]. For instance, pixel-based and object-based landslide detection methods have been explored by researchers such as [22–26] for traditional ML applications. The shift towards DL has been marked by studies from [27–33], among others. However, despite the adoption of ML and DL methods, the challenge of acquiring a substantial volume of labeled data for training these models persists, underscoring a critical bottleneck in the deployment of supervised learning techniques. To address this bottleneck, researchers have explored alternative methods that leverage geometrical, contextual, and/or topological information for landslide detection.

Methods such as the Contour Connection Method (CCM) and its adaptations, including the Scarp Identification and Contour Connection Method (SICCM), exemplify the innovative efforts to evaluate landslide features through geometrical and contextual information [34,35]. Their method focuses on the automated identification and classification of landslide deposits by analyzing terrain attributes derived from high-resolution LiDAR data. The approach involves the following key steps:

- Calculation of terrain derivatives such as slope, curvature, and roughness from the LiDAR DTM.
- Application of geometric criteria based on expert knowledge to identify potential landslide features. This includes thresholds on slope angles, curvature values, and other shape descriptors.
- Incorporation of contextual information, such as the proximity to known geological structures or land use data, to refine the detection results.
- Use of rule-based classification to categorize the identified features into landslide and non-landslide classes.

This method does not incorporate topological analysis but relies on predefined geometric and contextual rules derived from domain expertise. Several studies have employed alternative approaches. For example, methods such as those presented by [23,35] rely on pixel-based selection techniques combined with geometrical filters to detect landslides. These approaches typically involve image segmentation or thresholding based on spectral or terrain attributes to identify regions that potentially correspond to landslides. While these methods can be effective in certain contexts, they often depend heavily on the quality and resolution of the input data and may struggle to capture complex morphological features inherent to landslides.

In addition, ref. [36] have shown the feasibility of exploiting a layer of topological information by generating candidate polygons through PH, employing selective filters that consider only topological information. This approach, referred to as the Topological Method Using PH, leverages TDA to identify topological features associated with landslides. The key aspects of this method include:

- Computation of PH on the LiDAR-derived terrain data to capture topological signatures such as connected components and holes in the terrain.
- Identification of persistent topological features that may correspond to landslide regions without considering geometric or contextual attributes.
- Generation of landslide detection results based solely on topological properties derived from PH.

Unlike traditional methods, this approach does not use geometrical filters or contextual information, focusing entirely on the topological characteristics of the terrain to detect landslides. However, applying only topological information resulted in a notable incidence of false positives in certain contexts.

In response to these challenges, the recent literature has explored the potential of unsupervised learning approaches that circumvent the need for extensive labeled datasets. These methodologies focus on detecting landslides through the analysis of LiDAR or Digital Terrain Model (DTM) data, offering a promising avenue for identifying both recent and historical landslide events obscured by vegetation growth.

Building upon these insights, this paper introduces a novel approach that transcends traditional limitations by integrating topological, geometrical, and contextual information to detect geospatial objects, with a particular focus on landslides. This integration not only seeks to enhance detection accuracy but also aims to significantly reduce false positives, addressing the critical need for more sophisticated selective filters. By incorporating data from Light Detection and Ranging (LiDAR), NDVI, visual/near-infrared (NIR) satellite imagery, and additional geospatial sources, our method represents a paradigm shift in geospatial object detection strategies. The research question of this paper specifically focuses on the following:

Can filters based on combined topological, geometrical, and contextual information enhance the accuracy of topological knowledge-based geospatial object detection methods?

This advancement underscores the inadequacy of relying solely on topological data and highlights the potential benefits of a more holistic approach that synergizes multiple data dimensions. The integration of topological, geometrical, and contextual information marks the key novelty of our work, setting a new benchmark for precision and reliability in the detection of geospatial objects.

This study addresses these challenges by integrating PH with geometrical and contextual information to improve landslide detection accuracy. While prior research has applied PH in geospatial contexts, its use specifically for landslide detection remains limited [36]. Our approach leverages the persistent topological features extracted from LiDAR-derived DTM to identify candidate landslide regions. By combining topological insights with geometrical parameters (e.g., area, length–width ratio) and contextual factors (e.g., slope, vegetation index), we enhance the robustness of landslide detection against noise and variations in terrain. This integration represents an innovative contribution to the field, demonstrating how TDA and PH can be effectively applied to complex geospatial object detection problems.

This paper makes the following contributions:

- The development and evaluation of a topological knowledge-based (Topological KB) method for geospatial object detection that integrates topological, geometrical, and contextual information.
- The creation of a set of geometrical and contextual rules specifically tailored for landslide detection using the Topological KB method.
- An extensive analysis to pinpoint the most effective rule for landslide detection through rigorous experimentation with the established rule set.

The paper is structured as follows. Section 2 provides an overview of PH and geospatial object detection. Section 3 offers a comprehensive exploration of our method for geospatial object detection, which utilizes topological information combined with geometrical and contextual information. Section 4 details the study areas chosen for the experimentation and Section 5 discusses experimental procedures for detecting landslides. Section 6 presents the results and Section 7 discusses the findings from each study area. Finally, Section 8 provides concluding remarks.

2. Background

This section provides an overview of geospatial object detection as one of the tasks of geospatial data analysis and an overview for PH.

2.1. Knowledge-Based Object Detection

Geospatial object detection determines if a given geospatial dataset includes one or more geospatial objects belonging to the category of interest and locates their positions.

Different object detection methods exist and ref. [1] divides them into four categories: template matching-based, knowledge-based, object-based image analysis, and ML-based categories. Given that our proposed geospatial object detection method aligns with the knowledge-based category, this paper primarily focuses on explaining the knowledge-based object detection in more detail.

Knowledge-based object detection methods transform the geospatial object detection problem into the hypothesis-testing problem by creating different types of knowledge and rules [1]. There are two types of information on which hypothesis testing is based: geometrical and contextual information (Figure 1). Knowledge-based object detection methods employ geometrical information to encode prior knowledge into shape models. For example, farmlands have straight boundaries and specific sizes. Hence, one can hypothesize that this geometrical information, i.e., boundary properties and sizes, can be used to detect farmlands. Knowledge-based object detection methods that use contextual information employ relationships between geospatial objects and their background environment. In other words, contextual information is knowledge about how geospatial objects interact with their neighboring regions and other geospatial objects. One can hypothesize that landslides are located on a specific slope. Hence, the existence and degree of a slope can be utilized as a clue for landslide detection. For example, ref. [23] detected landslides by creating a rule that is based on prior knowledge about landslides. First, they identified candidate landslides, then performed a selection based on rules using geometrical and contextual information. It is worth noting that the main idea of knowledge-based object detection is to transform knowledge about detected geospatial objects into detection rules. On the one hand, if rules based on prior knowledge are too general, they will produce false-positive results. On the other hand, if rules are too specific, they will produce false-negative results [1].

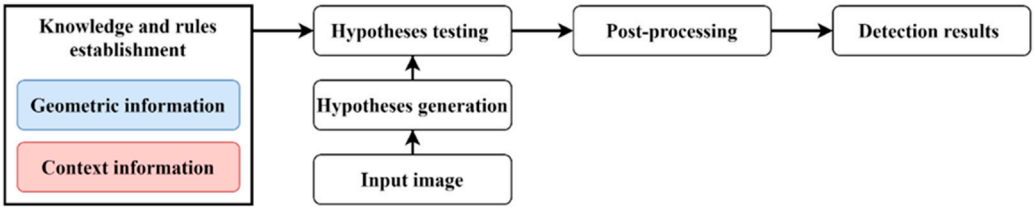


Figure 1. Knowledge-based object detection pipeline, adapted from [1].

2.2. Topological Data Analysis

TDA encompasses a collection of effective tools that can be used for the investigation and quantification of the shape and structure of datasets to answer questions in a specific domain [6]. Instead of using only statistical descriptors in the analysis, that can mislead when analyzing objects with different shapes [37], TDA seeks to analyze data in a fundamentally unique way by exploring the underlying shape [6]. Unlike traditional statistical methods that may overlook the shape-driven nuances of data, PH delves into spatial relationships and topological features across various scales, making it a pivotal tool for extracting deep insights. This approach not only enhances the understanding of data's inherent structure, but also opens new avenues for discovering patterns and relationships that are not immediately apparent through conventional analysis techniques [8].

PH is a tool used to extract topological insights from data by examining the links and gaps within the dataset [8]. PH takes advantage of the properties of simplicial complexes to extract topological data across different dimensions. A simplicial complex is a geometrical object built from simple pieces, called simplices. The simplest simplex is a point, or a 0-dimensional simplex. A 1-dimensional simplex is a line segment, a 2-dimensional simplex is a triangle, a 3-dimensional simplex is a tetrahedron, and so forth. Simplicial complexes are defined in a way that every face of a simplex in the complex is also a simplex in the complex, and the intersection of any two simplices in the complex is also a simplex in the complex. These properties of simplicial complexes allow for the mathematical study of

shapes and spaces through examining their homological features at different scales, which helps in identifying persistent features, the ones that persist over a range of scales [38]. To extract topological information from a specific dataset, [6] outlined a four-step process (Figure 2):

1. Regarding the PH tool, input a finite set of points with corresponding distance information [39]. The distance metric depends on the application, and the choice of the correct metric is essential. For example, protein data metrics can be measured in nanometers, and metrics for satellite image analysis can be measured in meters.
2. Construct a nested sequence of simplicial complexes from the set of points using different values of r.
3. Derive topological information from the nested sequence of simplicial complexes. This step consists of two functions:
   - Homology group returns topological information given the simplicial complex that was constructed using the r.
   - PH utilizes the homology group with a different value of r, and records each change. In other words, if the parameter r is changed, the topological information associated with the newly created simplicial complexes will change as well, and this second function records these changes.
4. Use the extracted topological information as a feature or descriptor for the dataset to assist in better understanding the dataset. This topological information can be visualized or can be a feature used in ML models.

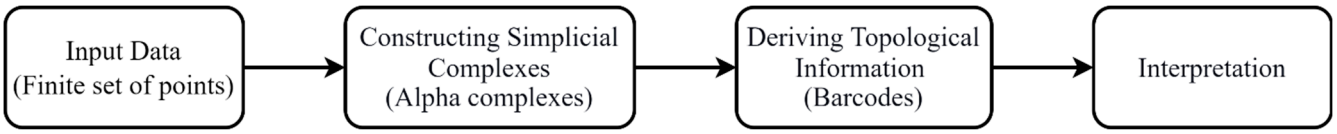


Figure 2. PH pipeline, adapted from [6].

In general, computing homology groups involves identifying holes in a specific dimension d in each oriented simplicial complex $\vec{K}$, where holes in dimension 0 are connected components [8]. To compute homology groups, two operations need to be performed. The first operation is identifying all cycles in the given chain group C_d. These cycles are identified by selecting simplices whose boundary is equal to 0 and defined as

$$Z_d = ker(\partial_d) = \{\sigma \in C_d(\vec{K}) | \partial(\sigma) = 0\} \quad (1)$$

In other words, all circles that exist in chain group $C_d(\vec{K})$ should be identified.

The second operation is identifying boundaries of $C_{d+1}(\vec{K})$, defined as

$$B_d = im(\partial_{d+1}) = \{\partial(\sigma | \ \sigma \in C_{d+1}(\vec{K}))\} \quad (2)$$

From the relation between Z_d and B_d, every element of B_d is an element of Z_d. B_d and Z_d contain all the necessary information to compute the holes in $\vec{K}$. Intuitively, the cycles that exist in $C_d(\vec{K})$ but are not the boundaries of $C_{d+1}(\vec{K})$ are holes in the d dimension of $\vec{K}$, which can be calculated using the following equation:

$$H_d = \frac{Z_d}{B_d} \quad (3)$$

Finally, to use outputs of the homology group, Betti numbers β that carry topological information need to be derived.

$$\beta_d(\vec{K}) = dim(H_d) \tag{4}$$

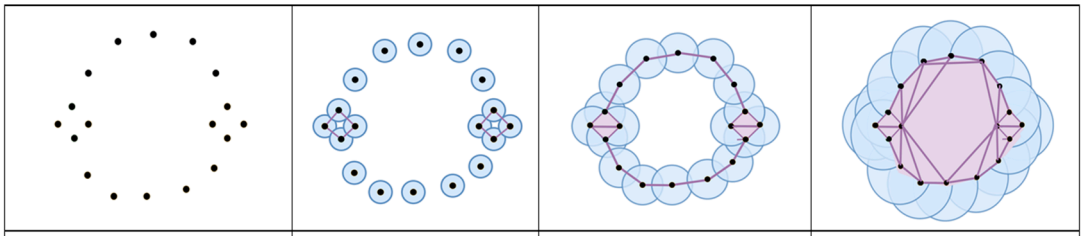
Betti number is the number of holes that exist in specific chain group C_d. For example, the Betti numbers from small dimensions have geometric interpretations:

$\beta_0(\vec{K})$: connected components;

$\beta_1(\vec{K})$: circles in two-dimensional space;

$\beta_2(\vec{K})$: voids in three-dimensional space.

The construction of simplicial complexes is dependent on the value of parameter r. If parameter r is equal to 0, every point is isolated (Figure 3a), and $\beta_0(\vec{K})$ will be equal to the number of points and $\beta_1(\vec{K})$ and $\beta_2(\vec{K})$ will be 0. With a large value of the parameter r, $\beta_0(\vec{K})$ will be 1 and every point will be connected (Figure 3d). Identifying the correct value of parameter r is vital to extract the topological information of the data. For example, in the set of points shown in Figure 3a, if parameter r is set to 1, two small circles are created (Figure 3b). However, if parameter r is set to 2, two small circles disappear, and one large circle is created. PH uses all possible values of parameter r and captures how the homology of the complexes $\vec{K}$ changes as the value of parameter r increases, and it detects the features that 'persist' across changes in the values of parameter r.



(**a**)	(**b**)	(**c**)	(**d**)
• $\vec{K}_1, r = 0$	• $\vec{K}_2$, r = 1	• $\vec{K}_3$, r = 2	• $\vec{K}_4, r = \infty$
• $\beta_0(\vec{K}) = 18$	• $\beta_0(\vec{K}) = 12$	• $\beta_0(\vec{K}) = 1$	• $\beta_0(\vec{K}) = 1$
• $\beta_1(\vec{K}) = 0$	• $\beta_1(\vec{K}) = 2$	• $\beta_1(\vec{K}) = 1$	• $\beta_1(\vec{K}) = 0$

Figure 3. A nested sequence of simplicial complex $\vec{K}$ illustrating the evolution of topological features with increasing radius r.

To track these changes, a nested sequence of simplicial complexes $\vec{K}$, called filtered simplicial complexes, is required, and can be defined as

$$\vec{K}_0 \subset \vec{K}_1 \subset \cdot \vec{K}_i \subset \vec{K}_j \subset \cdots \subset \vec{K}_l = \vec{K} \tag{5}$$

A filtration complex is a sequence of simplicial complexes generated by continuously increasing the parameter r (Figure 3). In other words, a series of VR or alpha complexes $\vec{K}_i$ with different values of the parameter r can be constructed from a set of points and can be defined as

$$0 \leq i \leq j \leq l$$

where l is the largest value of parameter r. Then, homology can be applied to record changes in Betti numbers β_d with function $f_{i,j}$, while the value of parameter r changes from i to j. The function can be written using the following equation:

$$f_{i,j} : H(\vec{K}_i) \rightarrow H(\vec{K}_j) \tag{6}$$

and this function records the following features:

Homology groups that are born at i;

Homology groups that persist from $i \rightarrow j$;

Homology groups that die at j.

Each homology class can be identified with a birth time and a death time. Features that are born and die soon after are often considered to be topological noise, whereas features that persist for an extended period are considered to be true features of the underlying structure (Figure 3c).

3. Methodology

3.1. Overview of the Topological Knowledge-Based (Topological KB) Method

We developed a Topological KB method where we use additional topological information along with geometrical and contextual information on candidate polygons derived from PH. The method is designed to tackle the above-mentioned research question by reframing the geospatial object detection challenge into a hypothesis testing problem. This transformation involves formulating various knowledge structures and rules using information about the detected geospatial object. Figure 4 illustrates the modification to the knowledge-based approach by [1] with the integration of topological information alongside geometrical and contextual information.

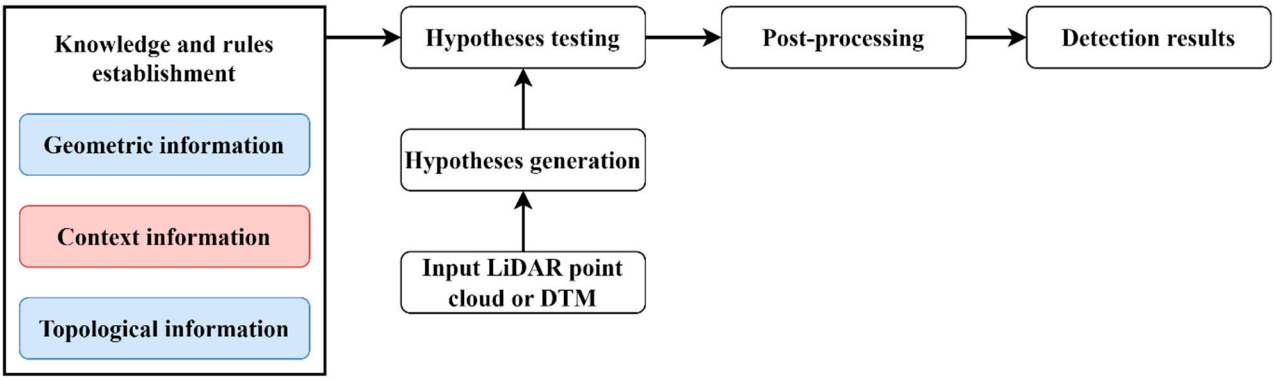


Figure 4. Topological KB method.

The application of PH in our method allows for the extraction of topological features that are inherently linked to the morphological characteristics of landslides. By computing the birth and death of topological features within the data, PH identifies persistent structures that correspond to landslide boundaries and shapes. These persistent features are used to generate candidate polygons, which are then subjected to further filtering. The use of PH ensures that the candidate polygons are not just based on superficial geometrical properties but are grounded in the fundamental topological signatures of landslides, improving the quality of the initial detection and reducing false positives.

Our method takes LiDAR-derived DTM data as the input; the process is illustrated in Figures 5 and 6 and in Algorithm 1. First, we extract LTFs from DTM and then, using PH, form candidate polygons from these LTFs. The last step involves applying rules for detection which are based on topological, geometrical, and contextual information.

Algorithm 1: Topological KB Method for Landslide Detection

Input:
LiDAR-derived DTM
Detection rules (geometrical and contextual parameters)
Output:
Detected landslide polygons
Steps:
Preprocessing:

Derive DTM from LiDAR point clouds with varying pixel sizes (e.g., 1 m, 5 m, 10 m).
Apply smoothing iterations to reduce noise (e.g., 0, 2, 5, 10, 15, 20 iterations).

1. Extraction of Linear Terrain Features (LTFs):
   1.1 Select an LTF extraction algorithm (e.g., Shade-relief, Curvature, Geomorphon).
   1.2 Apply the algorithm to the smoothed DTM to extract LTFs.
2. Creating Candidate Polygons using PH:
   2.1. Convert extracted LTFs into a set of points.
   2.2. Compute PH on the point set to obtain topological features.
      2.2.1. Use a filtration parameter to build simplicial complexes.
      2.2.2. Track birth and death times of topological features.
   2.3. Generate candidate polygons based on persistent topological features.
3. Feature Extraction:
   3.1. Compute geometrical features for each candidate polygon:
      3.1.1. Area
      3.1.2. Length–width ratio
   3.2. Compute contextual features for each candidate polygon:
      3.2.1. Slope
      3.2.2. Terrain Roughness Index (TRI)
      3.2.3. Normalized Difference Vegetation Index (NDVI)
   3.4. Apply topological filters:
      3.4.1. Filter based on birth time and lifetime of topological features.
   3.5. Apply geometrical filters:
      3.5.1. Filter based on area thresholds.
      3.5.2. Filter based on length–width ratio thresholds.
   3.6. Apply contextual filters:
      3.6.1. Filter based on slope range.
      3.6.2. Filter based on TRI range.
      3.6.3. Filter based on NDVI range.
   3.7. Retain candidate polygons that satisfy all detection rules.

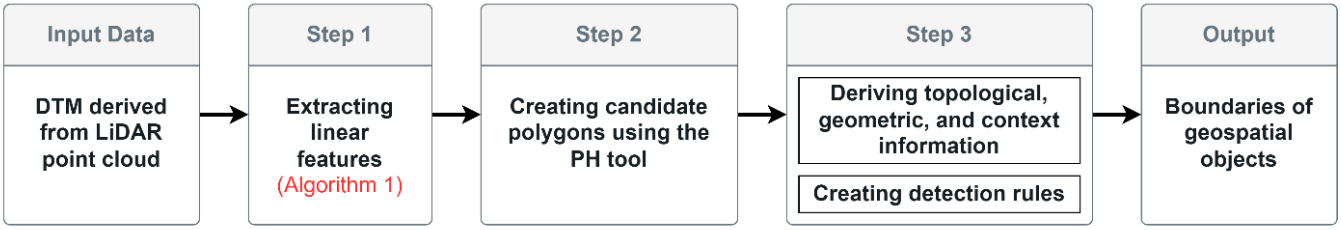
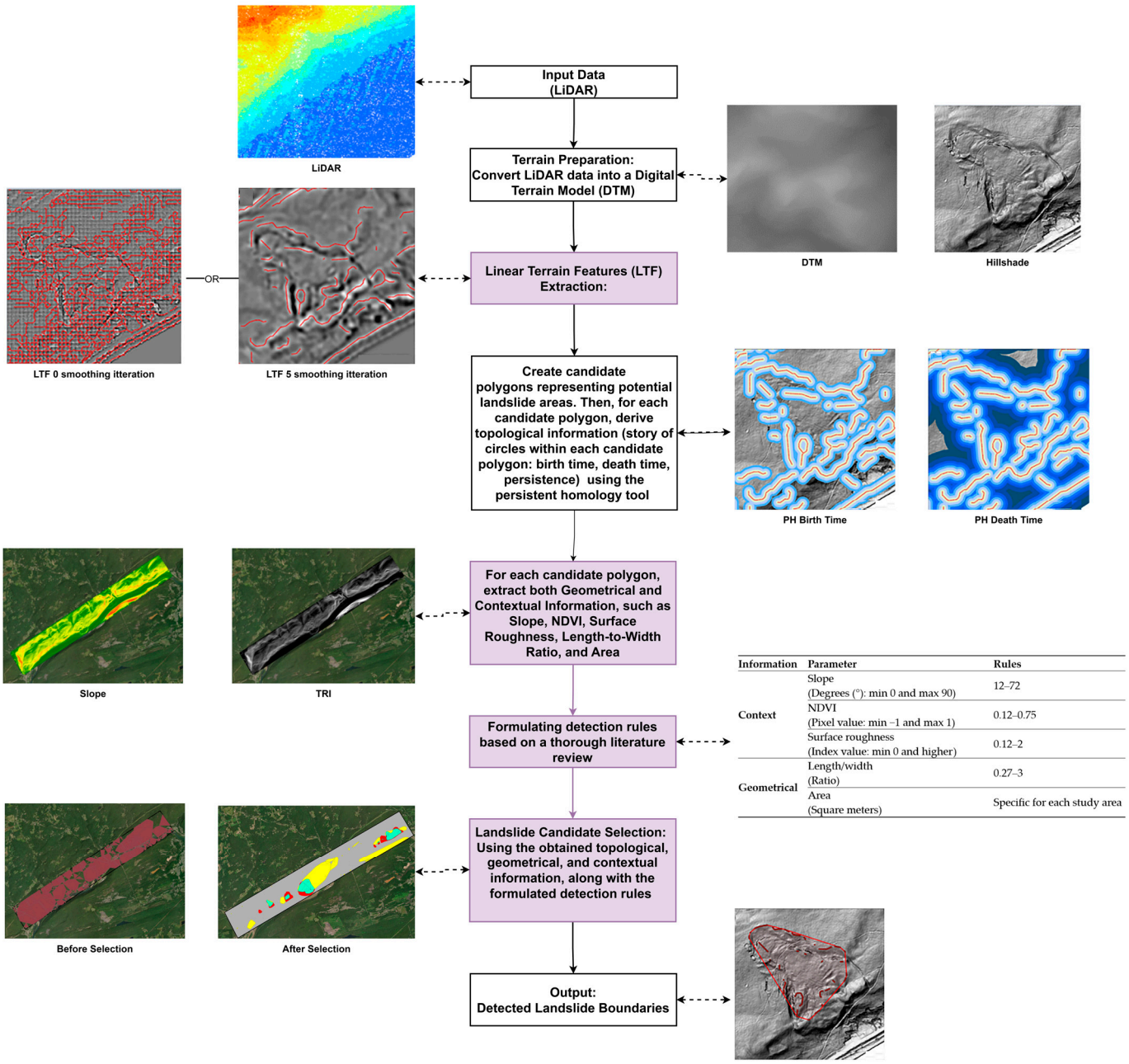


Figure 5. Workflow of the Topological KB geospatial object detection method.



Information	Parameter	Rules
Context	Slope (Degrees (°): min 0 and max 90)	12–72
	NDVI (Pixel value: min −1 and max 1)	0.12–0.75
	Surface roughness (Index value: min 0 and higher)	0.12–2
Geometrical	Length/width (Ratio)	0.27–3
	Area (Square meters)	Specific for each study area

Figure 6. Workflow of the Topological KB geospatial object detection method with visualization of each step.

3.2. Extracting Linear Terrain Features from DTM

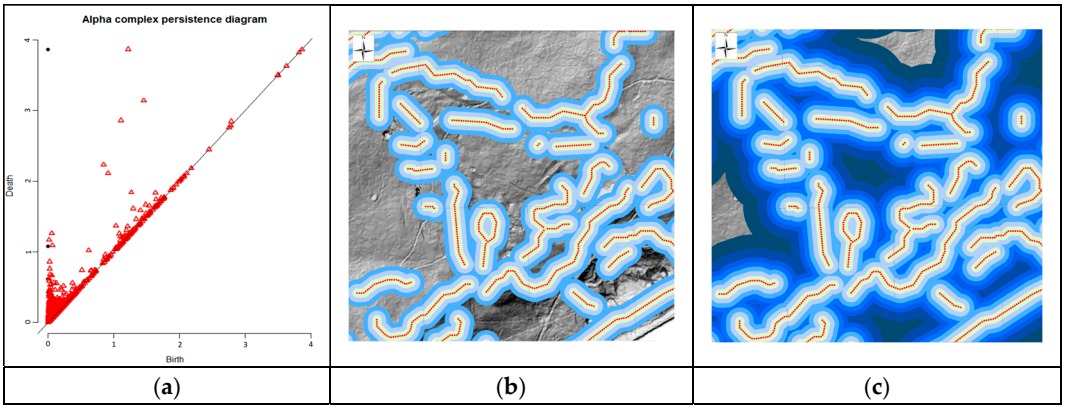
The process of extracting linear features, often referred to as "edge detection" or "line-finding", is frequently used in computer vision [40]. Linear features typically form the boundary lines between areas of different textures, intensities, or colors in an image. These lines usually highlight rapid intensity changes within a small region of the image and are crucial for conveying significant visual information such as shapes of objects. They often provide essential semantic cues related to surface alterations, depth transitions, changes in surface reflectance, and illumination discontinuities [40].

Morphological expressions of landslides can be characterized as a collection of small linear terrain features (LTFs) such as ridges and scarps and extracting them from DTM would identify landslide boundaries. Considerable research has been conducted on the detection of terrain morphology features including ridges and scarps. Rana (2006) proposed

a curvature-based semi-automated iterative channel and ridge identification algorithm that is simple and provides reliable results [41]. The algorithm can identify ridges and scarps but requires determination of a threshold value. Pirotti and Tarolli (2010) applied multiplication of the standard deviation as a threshold value to identify ridges and channels and developed an algorithm called "Curvature" [42]. Jasiewicz and Stepinski (2013) [43] proposed a new algorithm to identify landform elements called "Geomorphon". This algorithm does not require a threshold value and is based on the principle of pattern recognition [44]. Syzdykbayev et al. (2020) [44] proposed a new algorithm to identify landform elements called "Shade-relief". The Shade-relief algorithm is based on how humans analyze images to automate the extraction of LTFs directly from a DTM [44].

3.3. Creating Candidate Polygons Through PH

In the second step of the workflow, each of the LTFs was separately converted into a set of points and used as the input of PH. The output of PH is a set of points with topological information that includes the birth and death times of connected components and circles. This topological information is visualized in a PD, as presented in Figure 7a, and shows the birth time (Figure 7b, light blue) and death time (Figure 7c, dark blue) of the detected circle.



(**a**) (**b**) (**c**)

Figure 7. (**a**) Persistence diagram of the points: black dots represent features of dimension 0 (connected components), and red triangles represent features of dimension 1 (loops or cycles). (**b**) birth time (appearance) of the circles (light blue), and (**c**) death time of the circle (dark blue).

3.4. Using Topological, Geometrical, and Contextual Information for Detection Rules

Before formulating detection rules, it is essential to derive and embed topological, geometrical, and contextual information for each candidate polygon. We performed a comprehensive literature review to find works where the knowledge-based approach was used to detect landslides and compiled a list of landslide detection rules (Table 1). From this list, we selected and implemented the rules in each information category that are common in most works (Table 2).

The topological information, which can be obtained and embedded into candidate polygons using PH, includes

- The birth time of the circle, denoting the instance when topological information starts to emerge.
- The death time of the circle, denoting the moment when topological information ceases to exist.
- The lifetime of the circle, denoting the interval between the birth time and the death time.

Table 1. List of works on landslide detection rules.

Parameter	[45]	[23]	[46]	[47]	[48]	[49]	[50]	[51]	[52]	[53]	[35]	[54]
Slope (Degrees (°): min 0 and max 90)	>12	>10	10–60	>10	>15	>7	<72		>20.3	4–75	>30	>20
Hill shade (Pixel value: min 0 and max 255)	<92	<57.9										
Brightness (Pixel value: min 0 and max 255)	65 < 90	<40.1			$\mu - 2.5\sigma$	>104						>255
Elevation (Meters)	>30	>30				1600						
Curvature (Pixel value: min -1 and max 1)				−1&1							−1&1	
Surface roughness (Index value: min 0 and higher)				<2.4					>0.27		High	
Length (Meters)							6–61				<500	
Width (Meters)							6–20					
Length/width (Ratio)	>3	>3										>5
Stream order (8-bit pixel value: 0–255)	>5											
Distance from water body (Meters)	100	50										
Red band (8-bit pixel value: 0–255)	60–90	>64										
NIR band (8-bit pixel value: 0–255)								>255				
NDVI (Pixel value: min −1 and max 1)	>0.12	>0.18						>0.18	>0.176			<1

Table 2. List of geometrical and contextual rules implemented to detect landslides.

Information	Parameter	Rules	Derived Form	Justification
Context	Slope (Degrees (°): min 0 and max 90)	12–72	LiDAR	Landslides commonly occur within this slope range.
	NDVI (Pixel value: min −1 and max 1)	0.12–0.75	Satellite image	Indicates areas with sparse vegetation cover.
	Surface roughness (Index value: min 0 and higher)	0.12–2	LiDAR	Higher values suggest terrain irregularities.
Geometrical	Length/width (Ratio)	0.27–3	Candidate polygons	Reflects typical landslide shapes.
	Area (Square meters)	Specific for each study area	Candidate polygons	Based on known landslide sizes in study areas.

The birth time and lifetime of topological features derived from PH are crucial in distinguishing significant features from noise. Features with longer lifetimes are considered more meaningful as they persist across multiple scales [8]. We set a persistence threshold based on the distribution of feature lifetimes observed in our data. Features with lifetimes below this threshold were considered noise and filtered out. This approach aligns with methods used in TDA, where persistent features are indicative of underlying structural patterns.

Geometrical information, which can be obtained and embedded into candidate polygons using tools like Geographic Information Systems (GISs), includes

- Size, overall magnitude, or dimensions of a geospatial object. Landslides typically occupy a specific range of areas, depending on the terrain and geological conditions. We analyzed landslide inventories from our study areas and specified the area range for each study area.
- Ratio between length and width of a geospatial object—a measure of the object's proportion or aspect ratio. Landslides often exhibit elongated shapes due to the downhill movement of material. We set the length-to-width ratio threshold between 0.27 and 3, based on observations from previous studies [15] and an analysis of landslide shapes in our data. Polygons with ratios outside this range were considered less likely to represent landslides and were filtered out.

Contextual information, which can also be derived and embedded into candidate polygons using GIS tools, includes

- Slope of a region—the angle or steepness of the terrain. Slope is a critical factor in landslide susceptibility. Studies have shown that landslides commonly occur on slopes ranging from 12° to 72°. Slopes below 12° generally lack the gravitational force necessary to initiate landslides, while slopes above 72° are less stable and may result in rockfalls rather than soil-based landslides. We applied this slope range to focus on areas most prone to landslide activity.
- Roughness of a terrain—a measure of the terrain's irregularity or complexity. TRI measures the variability in elevation and is indicative of terrain complexity. Higher TRI values suggest rougher terrain, which can be associated with landslide scarps and deposits. We selected a TRI range of 0.12 to 2 based on the analysis of TRI values in known landslide areas within our study regions.
- NDVI score of a region—an indicator of live green vegetation density and health. NDVI values range from -1 to 1, with lower values indicating sparse vegetation and higher values indicating dense vegetation. Landslides can expose bare soil, resulting in lower NDVI values. We set an NDVI threshold between 0.12 and 0.75 to capture areas with reduced vegetation cover, which may correspond to recent landslide activity or zones susceptible to landslides.

4. Datasets

The characteristics of the input data for the experiments are shown in Table 3. A DTM offers a bare-Earth depiction of the terrain, devoid of natural or artificial elements such as vegetation or buildings. The output of the experiment, detected landslides, were compared against landslide inventory maps which record landslide locations along with supplementary data, including occurrence dates and landslide types [15].

The same five study areas described in [36] were used in the experiment (see Figure 8 and Table 3) and the characteristics of input data, both LiDAR and ground truth data with existing landslides, are described in Table 4.

Table 3. Characteristics of study areas.

	Study Area 1	Study Area 2	Study Area 3	Study Area 4	Study Area 5
Location (latitude, longitude)	41°12′39″N 76°03′44″W	45°34′0″N 123°11′0″W	39°10′44.6″N 107°50′58″W	45°42′0″N 122°53′0″W	47°36′28″N 122°20′6″W
State	Pennsylvania	Oregon	Colorado	Oregon	Washington
Area (Square meters)	25,572,981	135,587,076	167,225,478	134,963,016	216,603,450
Landslide Area (Square meters)	2,140,041	26,283,520	42,828,063	61,104,222	21,470,606
Percentage of Landslide Area	8.37%	19.38%	25.61%	45.27%	9.91%
Number of Landslides	7	738	206	1664	783
Elevation range (Meters)	From 151 to 471	From 48 to 548	From 1985 to 3174	From 7 to 521	From 0 to 159
Slope range (Degrees (°))	From 0 to 71.8	From 0 to 84.22	From 0 to 74.7	From 0 to 89.41	From 0 to 88.6

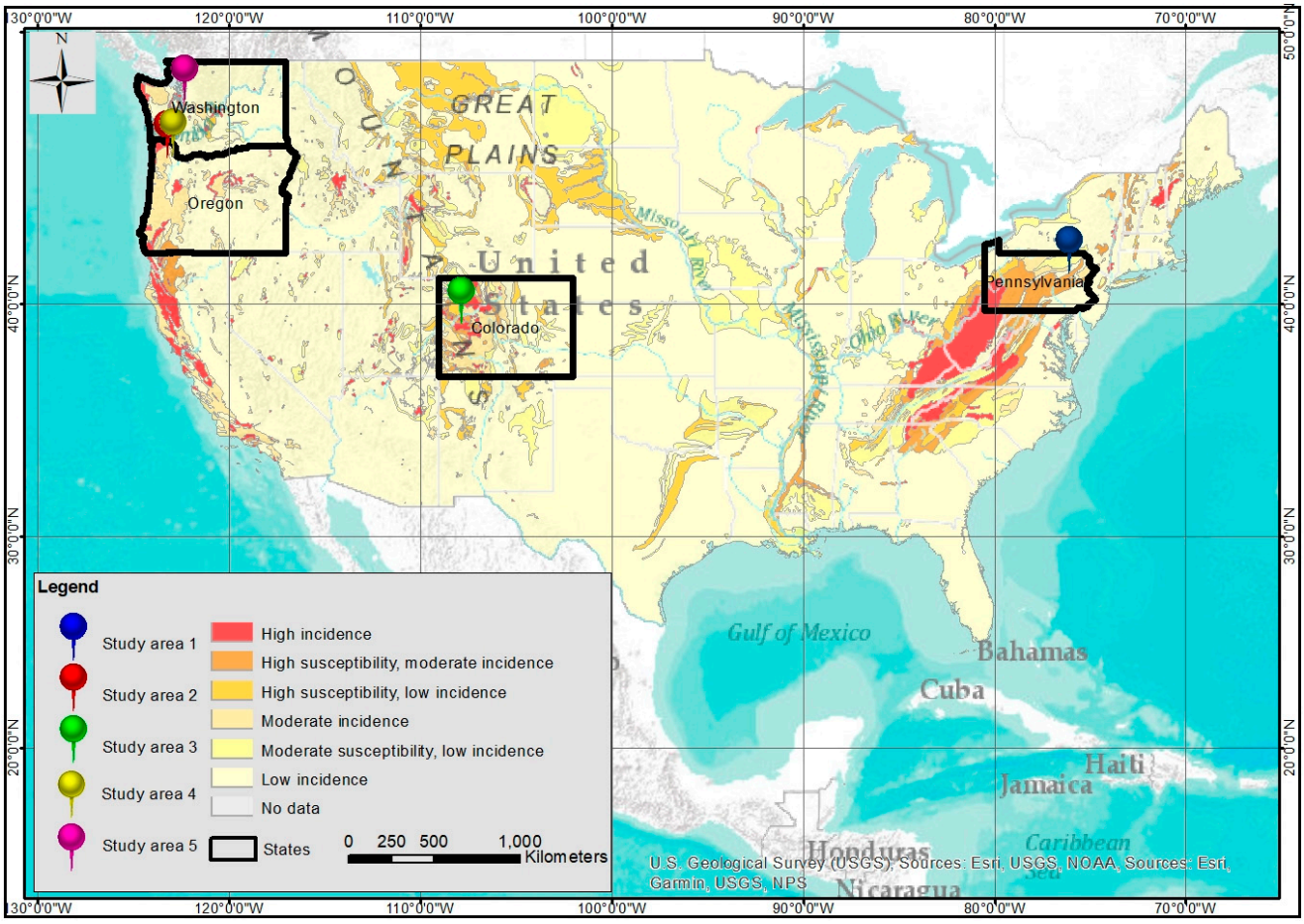


Figure 8. Landslide susceptibility maps in four states and for five study areas: Pennsylvania, Oregon, Colorado, and Washington.

Table 4. Characteristics of input data.

	Study Area 1	Study Area 2	Study Area 3	Study Area 4	Study Area 5
LIDAR (or LIDAR-derived DTM)					
Acquisition time	2006–2008	2007	2015–2016	2007	2000–2005
Source	Pennsylvania Spatial Data Access	State of Oregon Department of Geology and Mineral Industries	Colorado Geological Survey	State of Oregon Department of Geology and Mineral Industries	Puget Sound LiDAR Consortium
Horizontal ground resolution	1 m	1 m	1 m	1 m	1.8 m
Existing landslides (ground truth)					
Acquisition time	2019	2019	2015	2019	2017
Source	[55]	Gales Creek quadrangle Oregon's State-wide Landslide Information Database	Colorado Geological Survey	Dixie Mountain quadrangle Oregon's State-wide Landslide Information Database	Washington State Department of Natural Resources web portal
Acquisition method	Detecting visually LiDAR-derived DTM. Mimics protocol by [56].	Compiling landslide inventory data created by using LiDAR and protocol by [56].	Compiling landslide information digitized from 1:24 000-scale maps published in geologic hazard maps of Colorado.	Compiling landslide inventory data created by using LiDAR and protocol by [56].	Compiling landslide inventory data through different methods and scales.

5. Experiments

We conducted experiments to test our Topological KB. The results were evaluated by comparing them with the ground truth, the results of the work by [36], where only topological filters were used on candidate polygons, and the findings of the knowledge-based method implemented by [35] who introduced a method known as SICCM for landslide detection.

Three experiments were conducted as follows:

- Experiment 1: Using no filters—only raw, unfiltered candidate polygons.
- Experiment 2: Using only geometrical and contextual information as filters on candidate polygons.
- Experiment 3: Using topological information alongside geometrical and contextual information.

These experiments collectively provided a holistic view of the implications of different filtering approaches in the task of geospatial object detection.

To extract LTFs related to landslides, a LiDAR-derived DTM was used as input. As in any computer vision object detection task, the accuracy of any LTF extraction algorithm depends on the DTM pixel size. Another parameter is the number of smoothing iterations. With a high number of smoothing iterations, LTFs may be averaged out and treated as flat surfaces; without smoothing iterations, geospatial data noise in DTM can increase false-positive rates, resulting in extracting LTFs that do not exist (see Figure 9b1,c1).

We ran three LTF algorithms (Shade-relief, Curvature, and Geomorphon) on three different pixel sizes and used six smoothing iterations (Table 5). Furthermore, to identify the most effective geometrical and contextual information, we undertook a comprehensive analysis of all possible subsets. This analysis encompassed cases ranging from utilization of all possible combinations of geometrical and contextual information with and without the addition of topological information.

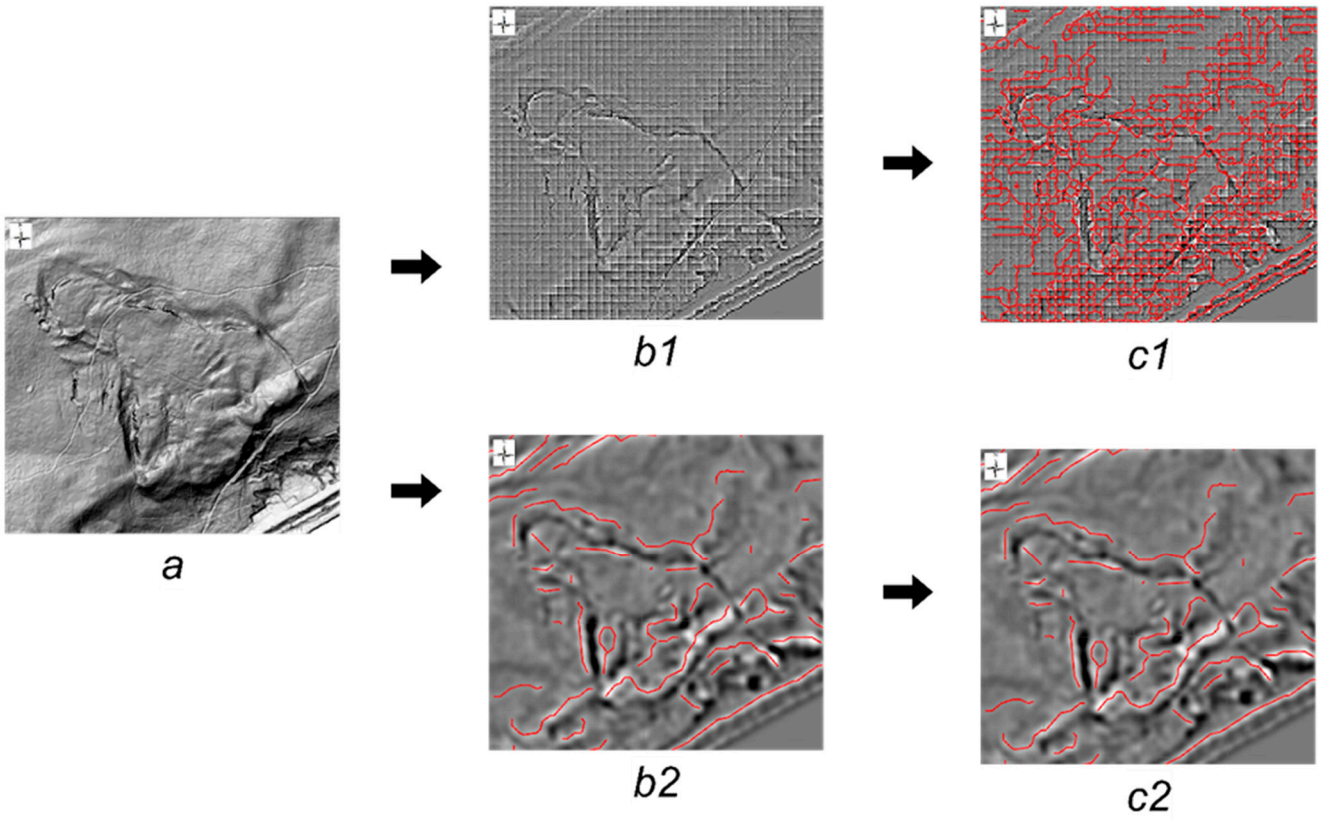


Figure 9. (**a**) Shaded relief surface; (**b1**) curvature of the surface with pixel size of 5 m; (**b2**) curvature of the surface with 5 times of smoothing iterations and with pixel size of 5 m; (**c1,c2**) extracted LTFs overlaying the curvature of the surface.

Table 5. Parameters used in the experiment.

Parameter Name	Parameters	Justification
DTM pixel size (Meters)	1, 5, 10	To assess the impact of spatial resolution on detection accuracy.
Smoothing iteration (Count)	0, 2, 5, 10, 15, 20	To determine the optimal level of noise reduction in DTM.
LTFs extraction algorithm	Shade-relief [44], Curvature [42], Geomorphon [43]	To compare the effectiveness of different feature extraction methods.
Topological information	Birth of the circle; lifetime of the circle.	Used birth time and lifetime as indicators of significant topological features.
Geometrical information	Min length–width ratio of the candidate polygon, max length–width ratio of the candidate polygon, min area, and max area.	Based on the literature and domain knowledge to identify typical characteristics of landslides.
Contextual information	Min slope, max slope, min TRI, max TRI, min NDVI, and max NDVI.	Based on the literature and domain knowledge to identify typical characteristics of landslides.

The total number of comparisons were 3 (LTFs extraction algorithm) × 3 (pixel size) × 6 (Smoothing iteration) × 4! (Geometrical information) × 6! (Contextual information) = 933,120.

6. Results

Detected landslides were compared to landslide inventory maps and with the results of the work by [36] in all five study areas. In addition, for Study Areas 2 and 4, the results were also compared with the results of the work by [35]. The three LTF extraction algorithms, six smoothing iterations, and different three-pixel sizes were applied, and accuracy, precision, recall, Cohen's kappa coefficient, and F-1 score evaluation metrics were calculated. Table 6 shows the results of these metrics with the highest F-1 score for each study area.

Table 6. Optimal performance metrics for Topological KB method across study areas.

	Study Area 1	**Study Area 2**	**Study Area 3**	**Study Area 4**	**Study Area 5**
LTFs extraction algorithm	Geomorphon	Geomorphon	Shade-relief	Curvature	Curvature
Pixel size (Meters)	1	1	1	5	5
Number of smoothing iterations (Count)	1	10	20	5	1
Accuracy	0.95	0.66	0.47	0.59	0.97
Precision	0.38	0.33	0.28	0.51	0.36
Recall	0.80	0.86	0.85	0.82	0.58
Cohen's kappa coefficient	0.50	0.31	0.12	0.24	0.43
F1 Score	0.52	0.48	0.43	0.64	0.45

The results on Table 6 demonstrate that our novel approach not only enhances the detection accuracy of landslides but also establishes a robust framework for minimizing false positives, thereby offering a substantial leap forward in the field of geospatial object detection.

Findings for Study Area 1

- Experiment 1: The best F1 score (0.34) was obtained with pixel sizes of five using Shade-relief (Figure 10b). Compared with [36], the unfiltered results were superior at pixel size 1 (Figure 10a) but deteriorated at pixel size 5 (Figure 10). Results with pixel size 10 lacked consistency across smoothing iterations (Figure 10c).
- Experiment 2: An F1-score peak of 0.5248 was observed at pixel size 1 using Geomorphon (Figure 10d). When compared with [36] the Topological KB geospatial object detection method outperformed in all configurations except for the pixel size of 10 subjected to 20 smoothing iterations (Figure 10d–f).
- Experiment 3: The highest F1 score was 0.5247, again at a pixel size of one (Figure 10g). Compared with [36], the Topological KB approach outperformed solely at pixel size 1 (Figure 10g–i).

In summary, the most favorable results for Study Area 1 were obtained when only geometrical and contextual filters were applied to a pixel size of one and with Geomorphon (Figure 10d). From the original set of 10 rules (comprising 4 geometrical and 6 contextual rules), a subset of 7 rules (consisting of 2 geometrical and 5 contextual rules) was chosen to attain these results (Table 7).

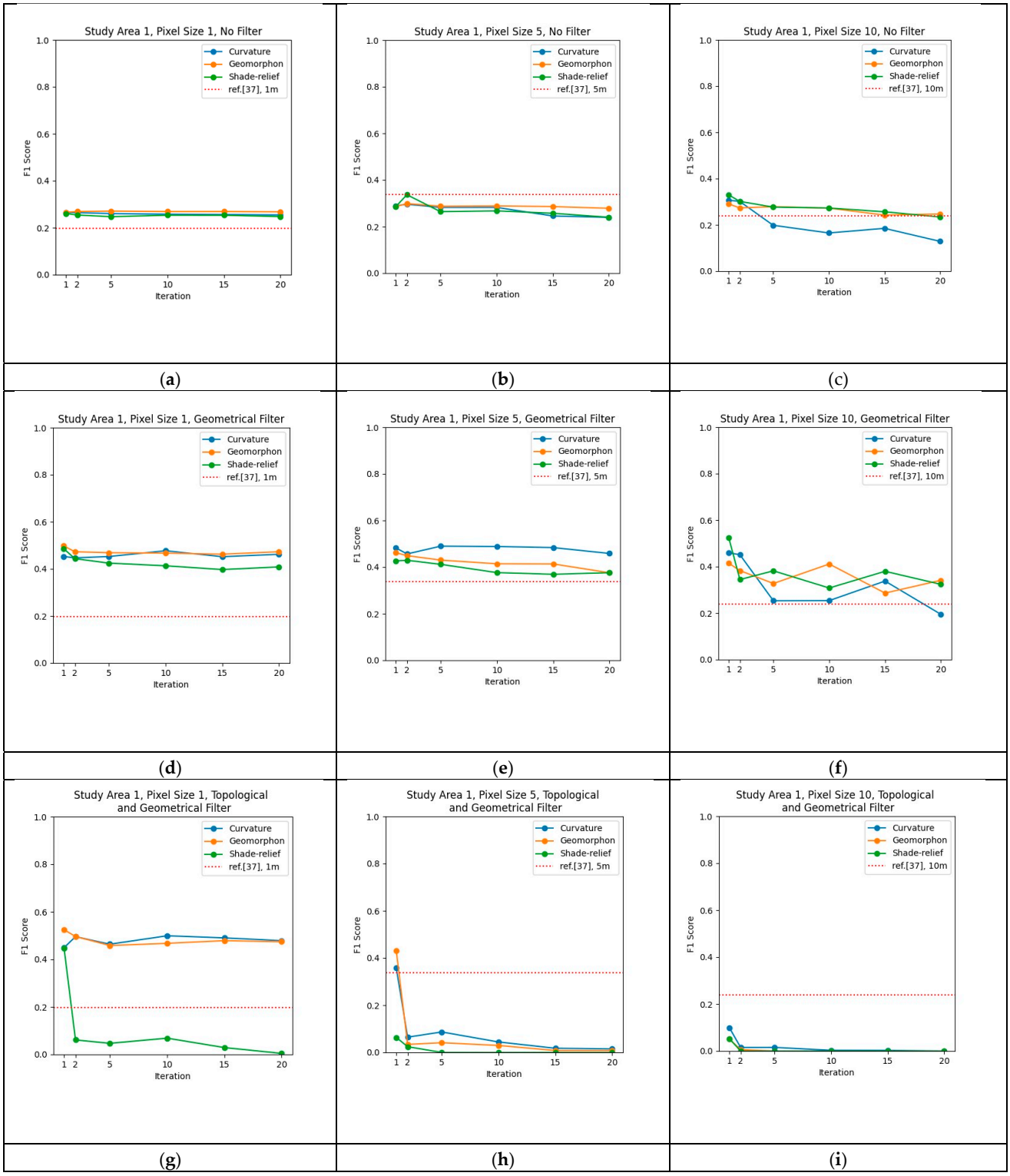


Figure 10. F1 scores for Study Area 1 (Pennsylvania) showing the results of the three experiments using different pixel sizes and smoothing iterations: (**a**–**c**) correspond to Experiment 1 (no filters applied), (**d**–**f**) correspond to Experiment 2 (geometrical and contextual filters applied), and (**g**–**i**) correspond to Experiment 3 (combined topological, geometrical, and contextual filters applied).

Table 7. List of geometrical and contextual rules used to obtain the highest F1 score; Study Area 1: Pennsylvania.

Information Type	Parameter	Rules	Rules Used
Context	Slope (Degrees (°): min 0 and max 90)	12–72	12–72
	NDVI (Pixel value: min −1 and max 1)	0.12–0.75	0.12–0.75
	Surface roughness (Index value: min 0 and higher)	0.12–2	0–2
Geometrical	Length/width (Ratio)	0.27–3	0–3
	Area (Square meters)	261–9,746,736	0–9,746,736

Findings for Study Area 2

- Experiment 1: The F1 score peaked at 0.39 with a pixel size of 10 using Curvature (Figure 11c). When compared with [35], F1 scores for the Topological KB geospatial object detection method was consistently lower across all pixel sizes (Figure 11a–c). Against [36], we observed reduced F1 scores at pixel sizes 1 and 5, while the results closely matched at pixel size 10 (Figure 11a–c).
- Experiment 2: The highest F1 score reached 0.48 at pixel size 1 with Geomorphon (Figure 11d). When compared with [35], results across all pixel sizes were closely matched, with a slight edge in the Topological KB geospatial object detection method in some instances (Figure 11d–f). Regarding [36], we matched their F1 scores at pixel sizes 1 and 5 but surpassed them at pixel size 10 (Figure 11d–f).
- Experiment 3: The highest F1 score was 0.47 at pixel size 10 using Geomorphon (Figure 11g). In comparison with both [35] and [36], the outcomes of the Topological KB geospatial object detection method were closely matched for pixel sizes 1 and 5 but lagged at pixel size 10 (Figure 11g–i).

In summary, the most favorable results for Study Area 2 were obtained when only geometrical and contextual filters were applied to pixel sizes of one and with Geomorphon (Figure 11d). From the original set of 10 rules (comprising 4 geometrical and 6 contextual rules), a subset of 5 rules (consisting of 1 geometrical and 4 contextual rules) was chosen to attain these results (Table 8).

Table 8. List of geometrical and contextual rules used to obtain the highest F1 score; Study Area 2: Oregon.

Information	Parameter	Rules	Rules Used
Context	Slope (Degrees (°): min 0 and max 90)	12–72	12–72
	NDVI (Pixel value: min −1 and max 1)	0.12–0.75	0–0.75
	Surface roughness (Index value: min 0 and higher)	0.12–2	0–2
Geometrical	Length/width (Ratio)	0.27–3	0–∞
	Area (Square meters)	261–12,443,892	261–∞

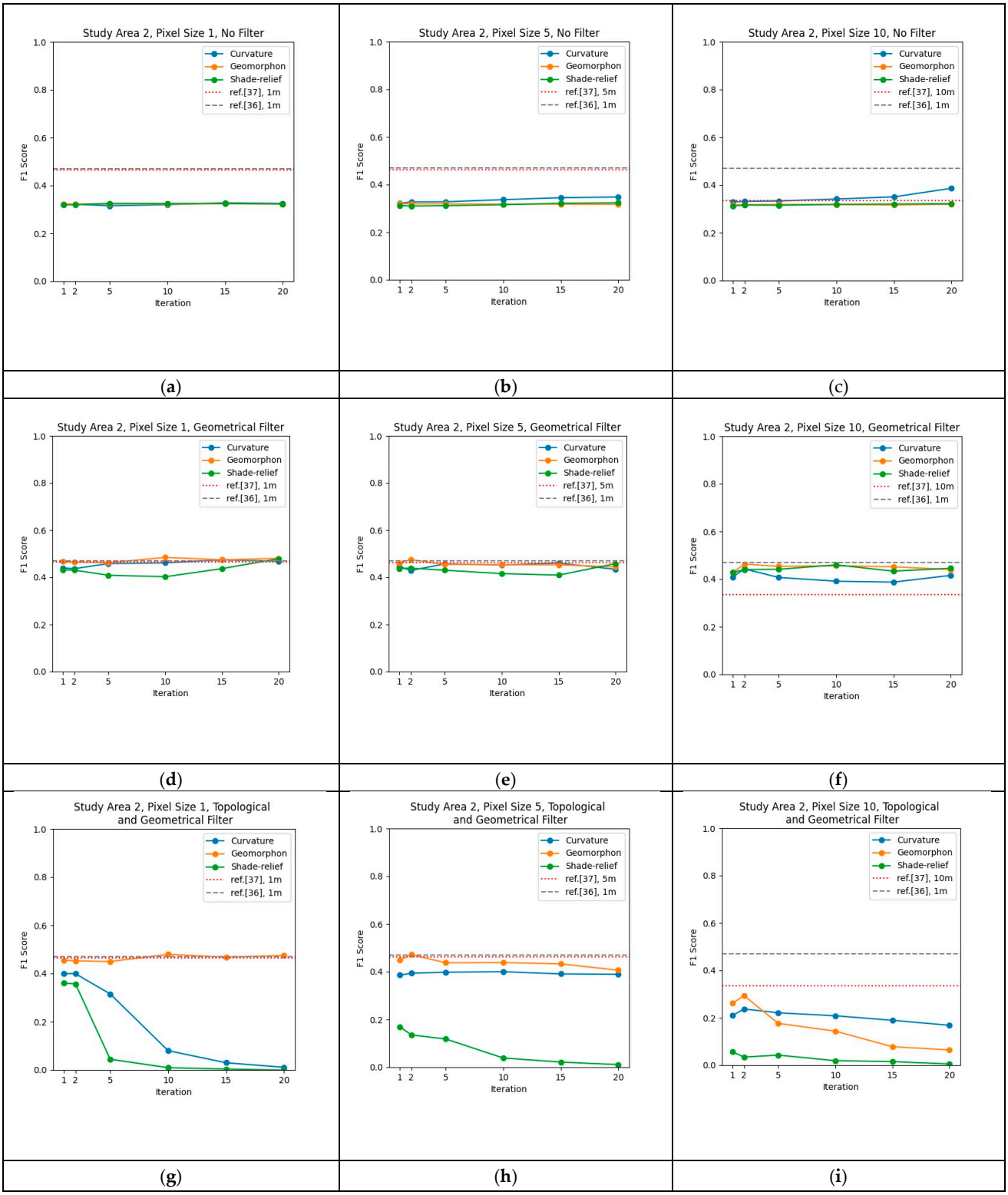


Figure 11. F1 scores for Study Area 2 (Oregon) showing the results of the three experiments using different pixel sizes and smoothing iterations: (**a**–**c**) correspond to Experiment 1 (no filters applied), (**d**–**f**) correspond to Experiment 2 (geometrical and contextual filters applied), and (**g**–**i**) correspond to Experiment 3 (combined topological, geometrical, and contextual filters applied).

Findings for Study Area 3

- Experiment 1: An optimal F1 score of 0.40 was achieved at pixel size 1 using Geomorphon (Figure 12a). Compared to [36], the absence of filters in this study showed improved results at pixel size 1 (Figure 12a–c).
- Experiment 2: The highest F1 score achieved was 0.43, observed at pixel size 1 when employing Shade-relief (Figure 12d). The results, in comparison with [36], indicated that using geometrical and contextual filters improved the results across all pixel sizes and smoothing iterations (Figure 12d–f).
- Experiment 3: The highest F1 score observed was 0.42 at pixel size 1 (Figure 12g). When compared with the results of [36], the use of the Topological KB method led to better results, but exclusively at pixel size 1 (Figure 12g–i).

In summary, the best results for Study Area 3 were achieved when only geometrical and contextual filters were applied to pixel sizes of one and with Shade-relief (Figure 12d). From the original set of 10 rules (comprising 4 geometrical and 6 contextual rules), a subset of 9 rules (consisting of 3 geometrical and 6 contextual rules) was chosen to attain these results (Table 9).

Table 9. List of geometrical and contextual rules used to obtain the highest F1 score; Study Area 3: Colorado.

Information	Parameter	Rules	Rules Used
Context	Slope (Degrees (°): min 0 and max 90)	12–72	0–72
	NDVI (Pixel value: min −1 and max 1)	0.12–0.75	0.12–0.75
	Surface roughness (Index value: min 0 and higher)	0.12–2	0.12–2
Geometrical	Length/width (Ratio)	0.27–3	0–3
	Area (Square meters)	1377–6,231,540	1377–6,231,540

Findings for Study Area 4

- Experiment 1: The optimal F1 score was 0.63 at pixel size 5 using Geomorphon (Figure 13b). Compared with [35], this experiment consistently yielded a higher F1 score across all cases. When compared with [36], the F1 score was lower for pixel sizes 1 and 10, but closely matched their results at pixel size 5 (Figure 13a–c).
- Experiment 2: The highest F1 score of 0.64 was observed at pixel size 5 using Curvature (Figure 13e). When compared with [35], the F1 score was higher across all pixel sizes. Compared with [36], the results indicated a lower F1 score at pixel sizes 1 and 10, while the score at pixel size 5 was almost identical to their findings (Figure 13d–f).
- Experiment 3: An F1 score of 0.63 was achieved at pixel size 1 using Geomorphon (Figure 13g). Compared with [35], the scores were higher for pixel sizes 1 and 5 but lower for pixel size 10. When compared with [36], the scores at pixel size 5 were similar, while the results for pixel sizes 1 and 10 were lower (Figure 13g–i).

In summary, the most favorable results for Study Area 4 were obtained when only geometrical and contextual filters were applied to pixel sizes of five and with Curvature (Figure 13e). From the original set of 10 rules (comprising 4 geometrical and 6 contextual rules), a subset of 5 rules (consisting of 2 geometrical and 3 contextual rules) was chosen to attain these results (Table 10).

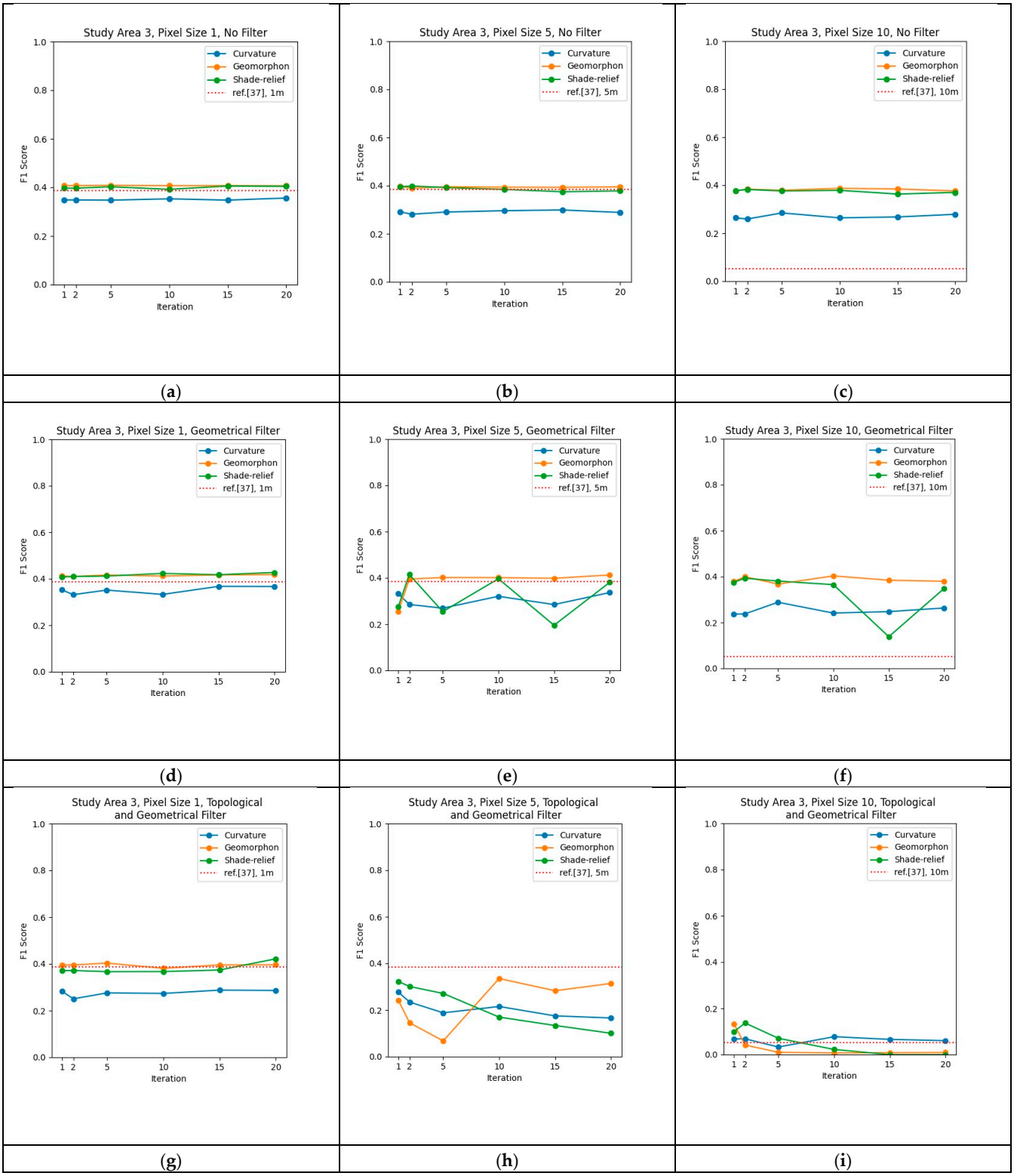


Figure 12. F1 scores for Study Area 3 (Colorado) showing the results of the three experiments using different pixel sizes and smoothing iterations: (**a**–**c**) correspond to Experiment 1 (no filters applied), (**d**–**f**) correspond to Experiment 2 (geometrical and contextual filters applied), and (**g**–**i**) correspond to Experiment 3 (combined topological, geometrical, and contextual filters applied).

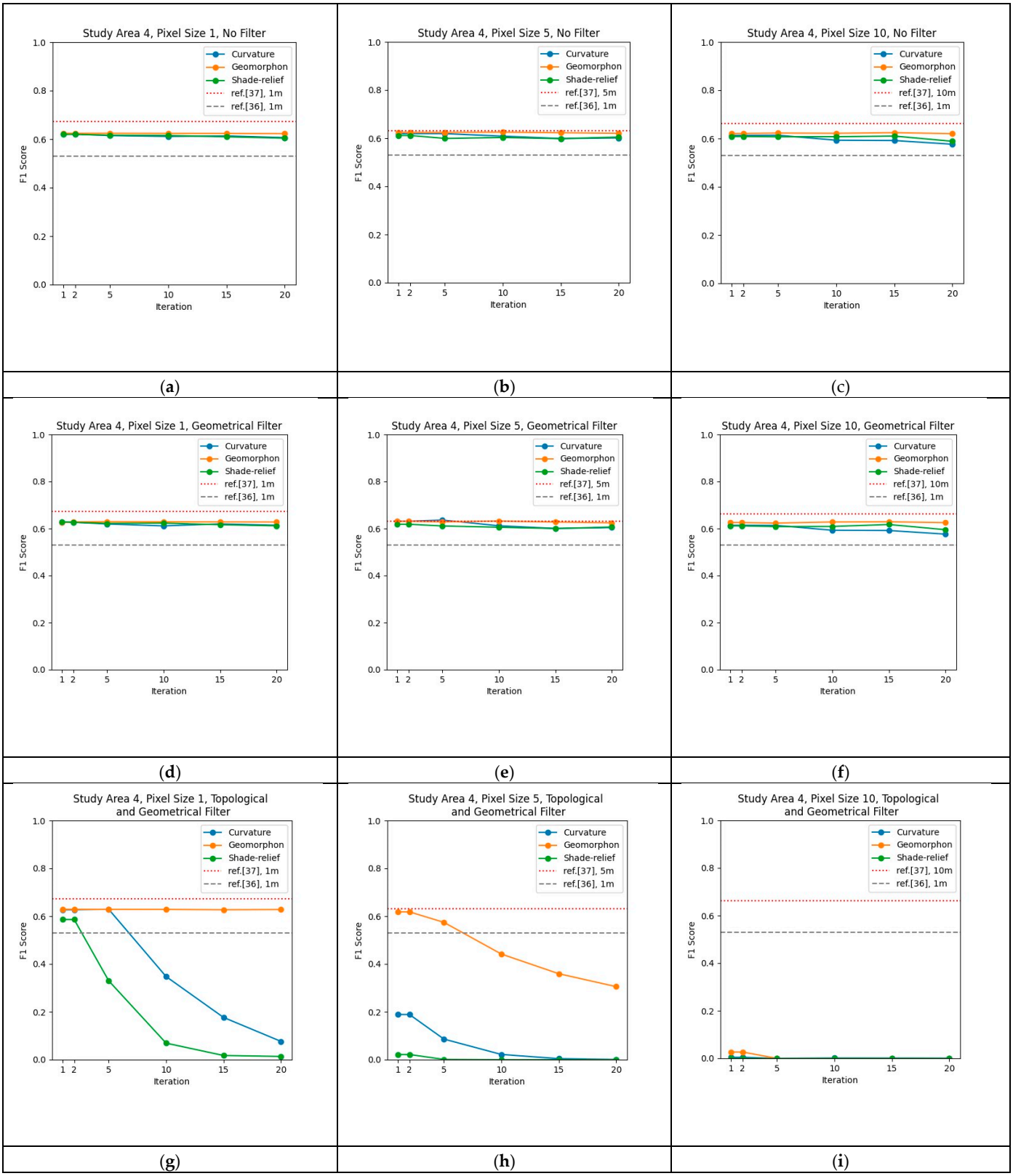


Figure 13. F1 scores for Study Area 4 (Oregon) showing the results of the three experiments using different pixel sizes and smoothing iterations: (**a**–**c**) correspond to Experiment 1 (no filters applied), (**d**–**f**) correspond to Experiment 2 (geometrical and contextual filters applied), and (**g**–**i**) correspond to Experiment 3 (combined topological, geometrical, and contextual filters applied).

Table 10. List of geometrical and contextual rules used to obtain the highest F1 score; Study Area 4: Oregon.

Information	Parameter	Rules	Rules Used
Context	Slope (Degrees (°): min 0 and max 90)	12–72	0–72
	NDVI (Pixel value: min −1 and max 1)	0.12–0.75	0–0.75
	Surface roughness (Index value: min 0 and higher)	0.12–2	0.12–∞
Geometrical	Length/width (Ratio)	0.27–3	0–3
	Area (Square meters)	18–314,297,870	0–314,297,870

Findings for Study Area 5

- Experiment 1: Optimal F1 scores of 0.07 were achieved with pixel sizes of 10 using Shade-relief. In comparison with [36], all results were inferior regardless of pixel size or smoothing iterations (Figure 14a–c).
- Experiment 2: The best F1 scores, reaching 0.45, were observed at pixel size 5, employing Curvature (Figure 14e). When compared with [36], the inclusion of geometrical and contextual filters resulted in enhanced outcomes across all pixel sizes and smoothing iterations (Figure 14d–f).
- Experiment 3: Peak F1 scores of 0.41 were observed at pixel size 1 with Curvature (Figure 14g). Compared with [36], the combined filtering approach led to improved results across all pixel sizes and smoothing iterations (Figure 14g–i).

In summary, the most favorable results for Study Area 5 were obtained when only geometrical and contextual filters were applied to pixel sizes of five and with Curvature (Figure 14e). From the original set of 10 rules (comprising 4 geometrical and 6 contextual rules), a subset of 4 rules (consisting of 1 geometrical and 3 contextual rules) was chosen to attain these results (Table 11).

Table 11. List of geometrical and contextual rules used to obtain the highest F1 score; Study Area 5: Washington.

Information	Parameter	Rules	Rules Used
Context	Slope (Degrees (°): min 0 and max 90)	12–72	12–72
	NDVI (Pixel value: min −1 and max 1)	0.12–0.75	0–0.75
	Surface roughness (Index value: min 0 and higher)	0.12–2	0–∞
Geometrical	Length/width (Ratio)	0.27–3	0–∞
	Area (Square meters)	137–5,689,077	0–5,689,077

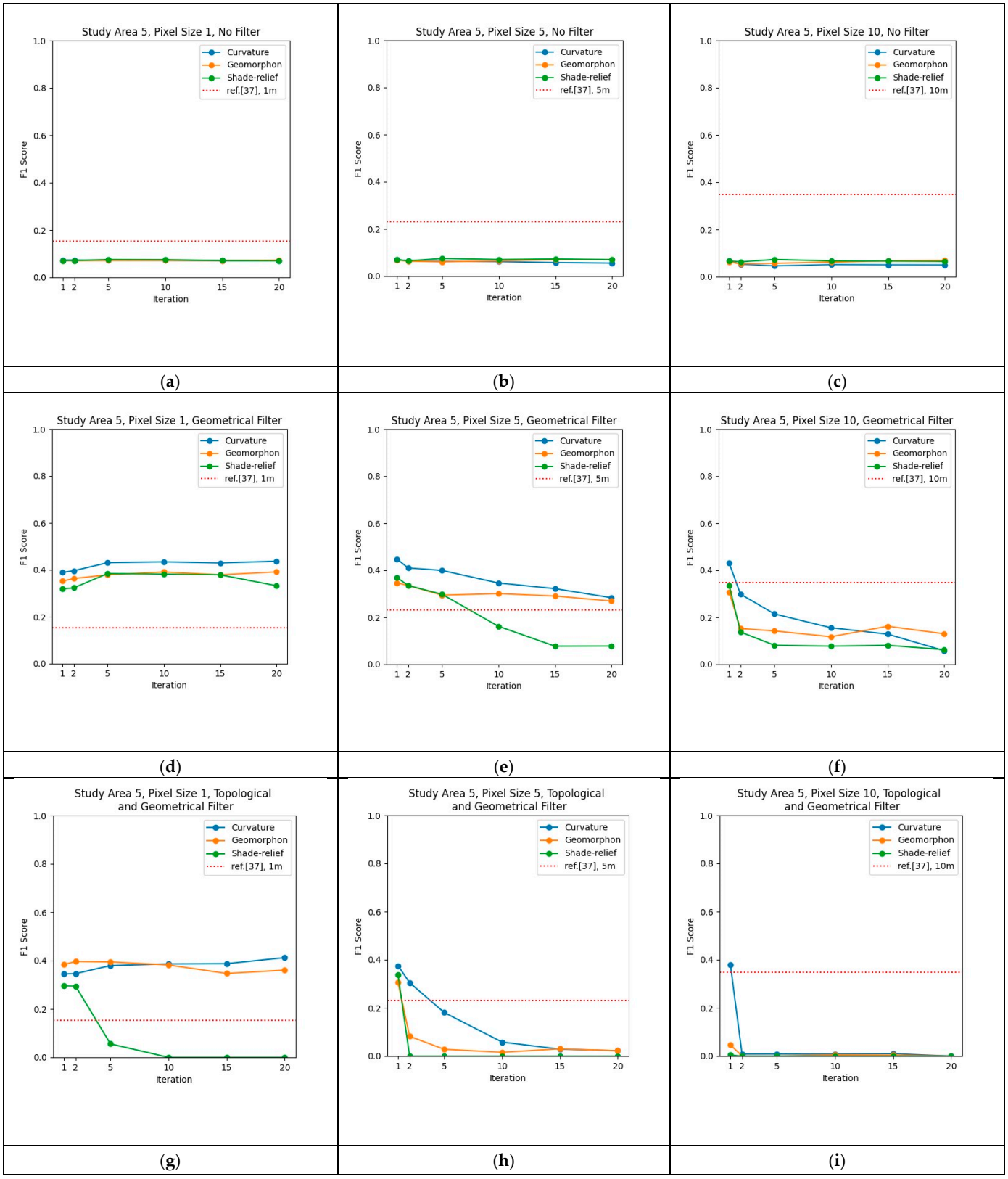


Figure 14. F1 scores for Study Area 5 (Washington) showing the results of the three experiments using different pixel sizes and smoothing iterations: (**a**–**c**) correspond to Experiment 1 (no filters applied), (**d**–**f**) correspond to Experiment 2 (geometrical and contextual filters applied), and (**g**–**i**) correspond to Experiment 3 (combined topological, geometrical, and contextual filters applied).

7. Discussion

Our analysis discerns a notable trend relating to pixel size and number of smoothing iterations: as the pixel size increases from 1 m to 10 m and the smoothing iterations are augmented, there is a corresponding decrease in the F1 score. This observation can be intuitively understood when considering the impact of increased pixel size and smoothing iterations on the quality and detail of the landslide boundary information. Increasing pixel size and number of smoothing iterations is analogous to reducing the resolution of the image or applying a strong blurring effect. In the context of geospatial object detection, this can be likened to examining a landscape from a greater distance or through a foggy lens. While larger pixel sizes and more smoothing iterations simplify the image and can aid in the detection of large-scale patterns or structures, they also hide the finer details that are often critical for accurate object detection. In the case of landslide detection, the intricate details of landslide boundaries, which often contain key indicators of landslide's characteristics and potentially its causes, are lost when viewed at lower resolutions. Consequently, while larger pixel sizes and increased smoothing iterations might expedite the processing and analysis of geospatial data, our results highlight the inherent trade-off between the simplification of data and the preservation of crucial details. Our findings underscore the importance of carefully selecting pixel size and the number of smoothing iterations in geospatial object detection tasks. Striking a balance between data simplification for efficiency and preservation of detail for accuracy is key to optimizing the results of such analyses.

Analyzing the results of the three sets of experiments conducted across the five study areas, we observe that Experiment 2, which uses filters based on geometrical and contextual information, consistently outperforms Experiment 1 (no filters) and Experiment 3 (which incorporates topological filters). The performance improvement in Experiment 2 is evident when considering the limitations of Experiment 1, where the absence of filters leads to a high risk of false positives. Without filtering, all polygons with a circular shape are identified as detected geospatial objects, resulting in an overestimation of the actual object count. While Experiment 3 introduces topological filters—specifically, the birth and lifespan of topological features like circles—these metrics correlate with the size of the circle, a characteristic already accounted for in the geometrical selection phase of Experiment 2. Consequently, Experiment 2 outperforms Experiment 3 in most cases, with few exceptions where their outcomes are comparable (as shown in Figure 12d,g).

Our analysis also reveals notable differences in detection accuracy across the five study areas, attributable to the unique geographical and environmental characteristics of each region. For instance, Study Area 1 (Pennsylvania) and Study Area 3 (Colorado) exhibited higher F1 scores when geometrical and contextual filters were applied, achieving scores of 0.52 and 0.45, respectively (see Table 6). These areas are characterized by homogeneous terrain and well-defined landslide features, which enhance the effectiveness of our method. In contrast, Study Areas 2 and 4 (both in Oregon) showed lower F1 scores, possibly due to complex terrain, dense vegetation cover, and the presence of smaller or less distinct landslides that are more challenging to detect. These variations underscore the impact of regional factors such as terrain complexity, vegetation density, and landslide morphology on the performance of geospatial object detection methods.

The integration of geometrical and contextual filters was pivotal in improving detection accuracy across all study areas. Geometrical filters based on area and length–width ratio allowed us to exclude candidate polygons that did not conform to the typical shape and size of landslides. Contextual filters utilizing slope, NDVI, and surface roughness further refined the results by aligning detected features with environmental conditions conducive to landslides. For example, in Study Area 4, the application of these filters resulted in the highest F1 score of 0.64, indicating that the combination of geometrical and contextual information effectively reduces false positives and enhances precision. This demonstrates that while topological features extracted via PH provide a robust foundation for identifying potential landslide regions, the integration of geometrical and contextual data is essential for accurately characterizing and confirming these regions as landslides.

Further analysis of our results reveals clear trends in how configuration parameters affect landslide detection performance. F1 scores tend to decrease as pixel size increases beyond 5 m, indicating that higher spatial resolution is crucial for capturing the detailed topological features of landslides. Similarly, increasing the number of smoothing iterations beyond a certain point leads to a drop in the F1 score, likely due to the over-smoothing of critical features necessary for accurate detection. Our findings also show that the choice of method significantly influences performance. The Shade-relief method excels at larger pixel sizes with fewer iterations. In contrast, the Geomorphon method performs best at finer resolutions, particularly under the topological and geometrical filter selection, highlighting the benefits of integrating topological information.

The adaptability and universality of our Topological KB method lie in its potential to detect a wide range of geospatial objects beyond landslides by leveraging topological properties derived from PH, coupled with domain-specific geometrical and contextual filters. By defining filters that capture the unique characteristics of the target object, the methodology can be tailored to various geospatial phenomena characterized by distinct topological signatures. For instance, in detecting sinkholes or volcanic craters, geometrical filters can identify circular depressions within specific size ranges, while contextual filters may include soil type and proximity to soluble rock formations. For urban feature detection, such as buildings or roads, geometrical filters could focus on linear or rectangular shapes, and contextual filters might incorporate land use data or proximity to infrastructure networks. This adaptability not only demonstrates the universality of our method but also suggests its potential to contribute to broader applications in geospatial analysis, including environmental monitoring, urban planning, and natural hazard assessment, provided that appropriate detection rules are established based on the unique properties of each target object.

Our comparative analysis with prior studies yields promising outcomes. When compared with the knowledge-based method utilized in the work by [35], our method shows superior results in both Study Areas 2 and 4 (Table 12). Similarly, when these results are compared against the results from the work by [36], which exclusively employed filters based only on topological information on candidate polygons, we observe an improvement in all study areas with one exception, Study Area 4. In Study Area 4, our results are closely aligned with the results of the work by [36]. The slight discrepancy underscores the inherent complexity of geospatial analysis and attests to the necessity of employing diverse, complementary strategies in different contexts to optimize outcomes (see Table 12).

Table 12. Results of Topological KB method [36] and [35] each study area.

	Study Area 1	**Study Area 2**	**Study Area 3**	**Study Area 4**	**Study Area 5**
Title	**Geospatial Object Detection: Topological KB Method**				
F1 score	0.52	0.48	0.43	0.64	0.45
Title	**Study [36]: Persistent homology on LiDAR data to detect landslides**				
F1 score	0.334	0.466	0.382	0.65	0.337
Title	**Study [35]: A simplified, object-based framework for efficient landslide inventorying using LIDAR digital elevation model derivatives**				
F1 score		0.47		0.53	

Our study builds upon the foundational work of [36] by integrating geometrical and contextual information such as area, height and width ratio, NDVI, slope, and surface roughness into the landslide detection framework, thereby extending the analysis beyond the primarily topological focus of the previous study. While the approach may seem similar in its use of PH for generating candidate polygons, our methodological enhancements through the incorporation of geometrical and contextual information present a more nuanced analysis of landslide susceptibility. This integration enables a more refined detection

of landslide features, particularly in complex terrains where topological information alone may not suffice (see Tables 6 and 12). The inclusion of geometrical and contextual information addresses the limitations of relying solely on topological data, offering a more comprehensive assessment of the factors influencing landslide occurrence. Consequently, our study not only validates the importance of topological features but also demonstrates the added value of incorporating environmental and geophysical parameters.

While advanced deep learning models often report high accuracy metrics, such as F1 scores exceeding 0.9, it is imperative to acknowledge the context and applicability of these results. Deep learning models require extensive labeled datasets for training, which may not always be available or feasible to obtain for every region prone to landslides. In contrast, our Topological KB method offers significant advantages in scenarios where labeled data are scarce or a rapid assessment is necessary following a landslide event. The method's reliance on readily available geospatial information and its capacity to integrate specific environmental features make it a valuable tool for initial assessments and in areas lacking detailed ground truth data.

Despite the promising results, our study has certain limitations. One major limitation is the dependency on the quality and resolution of input data. Variations in LiDAR data quality or the resolution of DTM can affect the extraction of topological features and, consequently, the accuracy of detection. Additionally, the detection rules, particularly the thresholds for geometrical and contextual filters, were derived from the specific characteristics of the study areas, raising concerns about the generalizability of the method to other regions with different geological or environmental conditions. The method may also be less effective in areas with dense vegetation cover, where landslide features are obscured, leading to potential under-detection. Furthermore, the reliance on predefined thresholds does not account for the full variability of landslide features, which may result in the omission of atypical landslides that do not conform to the established criteria.

To address these limitations and enhance the effectiveness of the Topological KB method, future research should focus on several areas. Incorporating adaptive thresholding or machine learning approaches could allow for the dynamic adjustment of detection rules based on regional characteristics, improving generalizability. Developing algorithms that automatically learn from labeled datasets could refine the selection of geometrical and contextual parameters, capturing a broader spectrum of landslide features. Integrating additional data sources, such as multi-temporal satellite imagery, could improve detection in vegetated areas by identifying changes over time that indicate landslide activity. Exploring the use of hyperspectral data or Synthetic Aperture Radar (SAR) imagery may provide further contextual information to enhance detection accuracy. Advanced SAR data processing techniques, such as the range ambiguity suppression scheme based on blind source separation, proposed by [57], could enhance the quality of SAR imagery for geospatial object detection. Combining SAR and LiDAR data may provide a more robust framework for detecting landslides across diverse environmental conditions.

Additionally, future investigations will explore the incorporation of more sophisticated geometrical features related to landslide characterization, drawing inspiration from recent studies such as those by [58–60]. By considering advanced geometrical descriptors and integrating them with environmental and geophysical parameters, our goal is to refine the detection and analysis of landslide features, particularly in complex terrains where traditional methods may fall short. Moreover, computational challenges associated with computing PH on large-scale geospatial datasets due to high dimensionality and data size must be addressed. Employing topology-preserving data reduction techniques, such as those proposed by [61], can optimize computations by reducing data complexity while maintaining essential topological features. Integrating such approaches could enhance the efficiency of our method, allowing for faster processing times without compromising accuracy.

8. Conclusions

This paper delves into the critical challenges of geospatial object detection amidst the burgeoning volume of geospatial data, emphasizing the imperative for more efficient processing methodologies. Central to our investigation is the hypothesis that the inclusion of topological information within a knowledge-based method significantly augments the accuracy of geospatial object detection compared to approaches that omit this information.

Our research demonstrates that the application of selective filters, grounded in geometrical and contextual insights, markedly improves object detection precision. Through a series of experiments focused on landslide detection using the Topological KB method, we discovered that while the amalgamation of geometrical and contextual information with topological features derived through PH enhances accuracy, the addition of further topological information does not yield additional accuracy gains. We meticulously developed and tested a set of geometrical and context-specific rules within our novel knowledge-based detection framework, identifying that rules emphasizing max slope and max NDVI are particularly impactful. These findings underscore their critical importance in enhancing methodological precision and reducing false positives across diverse geospatial contexts.

Despite the promising results, our study has certain limitations. One major limitation is the dependency on the quality and resolution of input data. Variations in LiDAR data quality or the resolution of DTM can affect the extraction of topological features and, consequently, the accuracy of detection. Additionally, the detection rules, particularly the thresholds for geometrical and contextual filters, were derived from the specific characteristics of the study areas. This raises concerns about the generalizability of the method to other regions with different geological or environmental conditions. The method may also be less effective in areas with dense vegetation cover, where landslide features are obscured, leading to potential under-detection. Furthermore, the reliance on predefined thresholds may result in the omission of atypical landslides that do not conform to established criteria.

To enhance the effectiveness of the Topological KB method, future research should focus on incorporating adaptive thresholding or machine learning approaches for the dynamic adjustment of detection rules based on regional characteristics, thereby improving generalizability. By refining the detection rules and integrating advanced geometrical descriptors with environmental and geophysical parameters, we aim to improve the universality and effectiveness of our approach in detecting various types of geospatial objects, particularly in complex terrains where traditional methods may fall short.

In essence, our findings substantiate that the strategic incorporation of geometrical and contextual information significantly contributes to the efficacy of geospatial object detection. However, the addition of new topological information, beyond that already encapsulated through PH in the detection process, does not further improve the accuracy of detecting geospatial objects. This conclusion, drawn from our comprehensive analysis using the Topological KB method for landslide detection, underscores the nuanced role of topological information in enhancing detection methodologies.

Author Contributions: Conceptualization, M.S. and H.A.K.; methodology, M.S.; writing—original draft preparation, M.S.; writing—review and editing, H.A.K.; visualization, M.S.; supervision, H.A.K. All authors have read and agreed to the published version of the manuscript.

Funding: This research received no external funding.

Data Availability Statement: The original contributions presented in the study are included in the article, further inquiries can be directed to the corresponding author.

Conflicts of Interest: The authors declare no conflicts of interest.

References

1. Cheng, G.; Han, J. A survey on object detection in optical remote sensing images. *ISPRS J. Photogramm. Remote Sens.* **2016**, *117*, 11–28. [CrossRef]
2. Pham, M.-T.; Courtrai, L.; Friguet, C.; Lefèvre, S.; Baussard, A. YOLO-Fine: One-Stage Detector of Small Objects Under Various Backgrounds in Remote Sensing Images. *Remote Sens.* **2020**, *12*, 2501. [CrossRef]

3. Pun, C.S.; Xia, K.; Lee, S.X. Persistent-Homology-Based Machine Learning and Its Applications—A Survey. *SSRN Electron. J.* **2018**. [CrossRef]
4. Zhou, L.; Pan, S.; Wang, J.; Vasilakos, A.V. Machine learning on big data: Opportunities and challenges. *Neurocomputing* **2017**, *237*, 350–361. [CrossRef]
5. Long, Y.; Gong, Y.; Xiao, Z.; Liu, Q. Accurate Object Localization in Remote Sensing Images Based on Convolutional Neural Networks. *IEEE Trans. Geosci. Remote Sens.* **2017**, *55*, 2486–2498. [CrossRef]
6. Chazal, F.; Michel, B. An Introduction to Topological Data Analysis: Fundamental and Practical Aspects for Data Scientists. *Front. Artif. Intell.* **2021**, *4*, 667963. [CrossRef]
7. Hensel, F.; Moor, M.; Rieck, B. A Survey of Topological Machine Learning Methods. *Front. Artif. Intell.* **2021**, *4*, 52. [CrossRef]
8. Otter, N.; Porter, M.A.; Tillmann, U.; Grindrod, P.; Harrington, H.A. A roadmap for the computation of persistent homology. *EPJ Data Sci.* **2017**, *6*, 1–38. [CrossRef]
9. Inatsu, M.; Kato, H.; Katsuyama, Y.; Hiraoka, Y.; Ohbayashi, I. A Cyclone Identification Algorithm with Persistent Homology and Merge-Tree. *SOLA* **2017**, *13*, 214–218. [CrossRef]
10. Feng, Z.; Li, H.; Zeng, W.; Yang, S.-H.; Qu, H. Topology Density Map for Urban Data Visualization and Analysis. *IEEE Trans. Vis. Comput. Graph.* **2020**, *27*, 828–838. [CrossRef]
11. Corcoran, P.; Jones, C.B. Topological data analysis for geographical information science using persistent homology. *Int. J. Geogr. Inf. Sci.* **2023**, *37*, 712–745. [CrossRef]
12. Bouchaffra, D.; Ykhlef, F. Persistent Homology for Land Cover Change Detection. In *Oxford Research Encyclopedia of Natural Hazard Science*; Oxford University Press: Oxford, UK, 2021.
13. Luo, W.; Liu, C.-C. Innovative landslide susceptibility mapping supported by geomorphon and geographical detector methods. *Landslides* **2017**, *15*, 465–474. [CrossRef]
14. Li, K.; Wan, G.; Cheng, G.; Meng, L.; Han, J. Object detection in optical remote sensing images: A survey and a new benchmark. *ISPRS J. Photogramm. Remote Sens.* **2020**, *159*, 296–307. [CrossRef]
15. Guzzetti, F.; Mondini, A.C.; Cardinali, M.; Fiorucci, F.; Santangelo, M.; Chang, K.-T. Landslide inventory maps: New tools for an old problem. *Earth-Sci. Rev.* **2012**, *112*, 42–66. [CrossRef]
16. Zhu, X.X.; Tuia, D.; Mou, L.; Xia, G.-S.; Zhang, L.; Xu, F.; Fraundorfer, F. Deep Learning in Remote Sensing: A Comprehensive Review and List of Resources. *IEEE Geosci. Remote Sens. Mag.* **2017**, *5*, 8–36. [CrossRef]
17. Rudari, R. Words into action guidelines: National Disaster Risk Assessment Hazard Specific Risk Assessment 4. Flood Hazard Risk Ass 2017. Available online: https://www.unisdr.org/files/globalplatform/591f213cf2fbe52828_wordsintoactionguideline.nationaldi.pdf (accessed on 3 August 2024).
18. Casagli, N.; Intrieri, E.; Tofani, V.; Gigli, G.; Raspini, F. Landslide detection, monitoring and prediction with remote-sensing techniques. *Nat. Rev. Earth Environ.* **2023**, *4*, 51–64. [CrossRef]
19. Hölbling, D.; Eisank, C.; Albrecht, F.; Vecchiotti, F.; Friedl, B.; Weinke, E.; Kociu, A. Comparing Manual and Semi-Automated Landslide Mapping Based on Optical Satellite Images from Different Sensors. *Geosciences* **2017**, *7*, 37. [CrossRef]
20. Highland, L.M.; Bobrowsky, P.T. *The Landslide Handbook—A Guide to Understanding Landslides*; US Geological Survey Circular: Reston, VA, USA, 2008. [CrossRef]
21. Tehrani, F.S.; Calvello, M.; Liu, Z.; Zhang, L.; Lacasse, S. Machine learning and landslide studies: Recent advances and applications. *Nat. Hazards* **2022**, *114*, 1197–1245. [CrossRef]
22. Gong, J.; Wang, D.; Li, Y.; Zhang, L.; Yue, Y.; Zhou, J.; Song, Y. Earthquake-induced geological hazards detection under hierarchical stripping classification framework in the Beichuan area. *Landslides* **2010**, *7*, 181–189. [CrossRef]
23. Martha, T.R.; Kerle, N.; van Westen, C.J.; Jetten, V.; Kumar, K.V. Segment Optimization and Data-Driven Thresholding for Knowledge-Based Landslide Detection by Object-Based Image Analysis. *IEEE Trans. Geosci. Remote Sens.* **2011**, *49*, 4928–4943. [CrossRef]
24. Stumpf, A.; Kerle, N. Object-oriented mapping of landslides using Random Forests. *Remote Sens. Environ.* **2011**, *115*, 2564–2577. [CrossRef]
25. Eeckhaut, M.V.D.; Poesen, J.; Verstraeten, G.; Vanacker, V.; Moeyersons, J.; Nyssen, J.; van Beek, L. The effectiveness of hillshade maps and expert knowledge in mapping old deep-seated landslides. *Geomorphology* **2004**, *67*, 351–363. [CrossRef]
26. Eeckhaut, M.V.D.; Kerle, N.; Poesen, J.; Hervás, J. Object-oriented identification of forested landslides with derivatives of single pulse LiDAR data. *Geomorphology* **2012**, *173*, 30–42. [CrossRef]
27. Can, R.; Kocaman, S.; Gokceoglu, C. A convolutional neural network architecture for auto-detection of landslide photo-graphs to assess citizen science and volunteered geographic information data quality. *ISPRS Int. J. Geoinf.* **2019**, *8*, 300. [CrossRef]
28. Ding, A.; Zhang, Q.; Zhou, X.; Dai, B. Automatic recognition of landslide based on CNN and texture change detection. In Proceedings of the 2016 31st Youth Academic Annual Conference of Chinese Association of Automation (YAC), Wuhan, China, 11-13 November 2016; IEEE: New York, NY, USA, 2016; pp. 444–448.
29. Ghorbanzadeh, O.; Blaschke, T. Optimizing Sample Patches Selection of CNN to Improve the mIOU on Landslide Detec-tion. In Proceedings of the 5th International Conference on Geographical Information Systems Theory, Applications and Management (GISTAM 2019), Heraklion, Crete Greece, 3–5 May 2019; pp. 33–40.
30. Ghorbanzadeh, O.; Blaschke, T.; Gholamnia, K.; Meena, S.R.; Tiede, D.; Aryal, J. Evaluation of Different Machine Learning Methods and Deep-Learning Convolutional Neural Networks for Landslide Detection. *Remote Sens.* **2019**, *11*, 196. [CrossRef]

31. Pham, B.T.; Tien Bui, D.; Prakash, I.; Dholakia, M.B. Hybrid integration of Multilayer Perceptron Neural Networks and machine learning ensembles for landslide susceptibility assessment at Himalayan area (India) using GIS. *Catena* **2017**, *149*, 52–63. [CrossRef]
32. Prakash, N.; Manconi, A.; Loew, S. Mapping landslides on EO data: Performance of deep learning models vs. traditional machine learning models. *Remote Sens.* **2020**, *12*, 346. [CrossRef]
33. Oak, O.; Nazre, R.; Naigaonkar, S.; Sawant, S.; Vaidya, H. A Comparative Analysis of CNN-based Deep Learning Models for Landslide Detection. *arXiv* **2024**, arXiv:2408.01692.
34. Leshchinsky, B.A.; Olsen, M.J.; Tanyu, B.F. Contour Connection Method for automated identification and classification of landslide deposits. *Comput. Geosci.* **2015**, *74*, 27–38. [CrossRef]
35. Bunn, M.D.; Leshchinsky, B.A.; Olsen, M.J.; Booth, A. A Simplified, Object-Based Framework for Efficient Landslide Inventorying Using LIDAR Digital Elevation Model Derivatives. *Remote Sens.* **2019**, *11*, 303. [CrossRef]
36. Syzdykbayev, M.; Karimi, B.; Karimi, H.A. Persistent homology on LiDAR data to detect landslides. *Remote Sens. Environ.* **2020**, *246*, 111816. [CrossRef]
37. Matejka, J.; Fitzmaurice, G. Same stats, different graphs: Generating datasets with varied appearance and identical statistics through simulated annealing. In Proceedings of the 2017 CHI Conference on Human Factors in Computing Systems, Denver, CO, USA, 6–11 May 2017; pp. 1290–1294.
38. Salnikov, V.; Cassese, D.; Lambiotte, R. Simplicial complexes and complex systems. *Eur. J. Phys.* **2018**, *40*, 014001. [CrossRef]
39. Carlsson, G. Topology and data. *Bull. Am. Math. Soc.* **2009**, *46*, 255–308. [CrossRef]
40. Szeliski, R. *Computer Vision: Algorithms and Applications*; Springer Science & Business Media: New York, NY, USA, 2010.
41. Rana, S. Use of plan curvature variations for the identification of ridges and channels on DEM. In *Progress in Spatial Data Handling—12th International Symposium on Spatial Data Handling*; SDH 2006; Springer: Berlin/Heidelberg, Germany, 2006. [CrossRef]
42. Pirotti, F.; Tarolli, P. Suitability of LiDAR point density and derived landform curvature maps for channel network extraction. *Hydrol. Process.* **2010**, *24*, 1187–1197. [CrossRef]
43. Jasiewicz, J.; Stepinski, T.F. Geomorphons—A pattern recognition approach to classification and mapping of landforms. *Geomorphology* **2013**, *182*, 147–156. [CrossRef]
44. Syzdykbayev, M.; Karimi, B.; Karimi, H.A. A Method for Extracting Some Key Terrain Features from Shaded Relief of Digital Terrain Models. *Remote Sens.* **2020**, *12*, 2809. [CrossRef]
45. Martha, T.R.; Kerle, N.; Jetten, V.; van Westen, C.J.; Kumar, K.V. Characterising spectral, spatial and morphometric prop-erties of landslides for semi-automatic detection using object-oriented methods. *Geomorphology* **2020**, *116*, 24–36. [CrossRef]
46. Hölbling, D.; Füreder, P.; Antolini, F.; Cigna, F.; Casagli, N.; Lang, S. A Semi-Automated Object-Based Approach for Landslide Detection Validated by Persistent Scatterer Interferometry Measures and Landslide Inventories. *Remote Sens.* **2012**, *4*, 1310–1336. [CrossRef]
47. Liu, J.-K.; Hsiao, K.-H.; Shih, P.T.-Y. A geomorphological model for landslide detection using airborne LIDAR data. *J. Mar. Sci. Technol.* **2012**, *20*, 4.
48. Rau, J.-Y.; Jhan, J.-P.; Rau, R.-J. Semiautomatic object-oriented landslide recognition scheme from multisensor optical im-agery and DEM. *IEEE Trans. Geosci. Remote Sens.* **2013**, *52*, 1336–1349. [CrossRef]
49. Blaschke, T.; Feizizadeh, B.; Holbling, D. Object-Based Image Analysis and Digital Terrain Analysis for Locating Landslides in the Urmia Lake Basin, Iran. *IEEE J. Sel. Top. Appl. Earth Obs. Remote Sens.* **2014**, *7*, 4806–4817. [CrossRef]
50. Althuwaynee, O.F.; Pradhan, B.; Park, H.-J.; Lee, J.H. A novel ensemble bivariate statistical evidential belief function with knowledge-based analytical hierarchy process and multivariate statistical logistic regression for landslide susceptibility map-ping. *Catena* **2014**, *114*, 21–36. [CrossRef]
51. Hong, H.; Pradhan, B.; Xu, C.; Bui, D.T. Spatial prediction of landslide hazard at the Yihuang area (China) using two-class kernel logistic regression, alternating decision tree and support vector machines. *Catena* **2015**, *133*, 266–281. [CrossRef]
52. Mezaal, M.R.; Pradhan, B.; Sameen, M.I.; Shafri, H.Z.M.; Yusoff, Z.M. Optimized Neural Architecture for Automatic Landslide Detection from High-Resolution Airborne Laser Scanning Data. *Appl. Sci.* **2017**, *7*, 730. [CrossRef]
53. Fanos, A.; Pradhan, B.; Mansor, S.; Yusoff, Z.M.; bin Abdullah, A.F. A hybrid model using machine learning methods and GIS for potential rockfall source identification from airborne laser scanning data. *Landslides* **2018**, *15*, 1833–1850. [CrossRef]
54. Bacha, A.S.; Van Der Werff, H.; Shafique, M.; Khan, H. Transferability of object-based image analysis approaches for landslide detection in the Himalaya Mountains of northern Pakistan. *Int. J. Remote Sens.* **2020**, *41*, 3390–3410. [CrossRef]
55. Karimi, B.; Karimi, H.A. An automated method for the detection of topographic patterns at tectonic boundaries. In Proceedings of the The Ninth International Conferences on Pervasive Patterns and Applications, Athens, Greece, 19–23 February 2017; pp. 72–77.
56. Burns, W.J.; Maidin, I.P.; Ma, L. Statewide Landslide Information Database for Oregon (SLIDO), Release 1. In Proceedings of the 2008 Joint Meeting of The Geological Society of America, Soil Science Society of America, American Society of Agronomy, Crop Science Society of America, Gulf Coast Association of Geological Societies with the Gulf Coast Section of SEPM, Houston, TX, USA, 5–9 October 2008.
57. Chang, S.; Deng, Y.; Zhang, Y.; Zhao, Q.; Wang, R.; Zhang, K. An Advanced Scheme for Range Ambiguity Suppression of Spaceborne SAR Based on Blind Source Separation. *IEEE Trans. Geosci. Remote Sens.* **2022**, *60*, 5230112. [CrossRef]
58. Amato, G.; Palombi, L.; Raimondi, V. Data–driven classification of landslide types at a national scale by using Artificial Neural Networks. *Int. J. Appl. Earth Obs. Geoinf.* **2021**, *104*, 102549. [CrossRef]

59. Rana, K.; Ozturk, U.; Malik, N. Landslide Geometry Reveals its Trigger. *Geophys. Res. Lett.* **2021**, *48*, e2020GL090848. [CrossRef]
60. Taylor, F.E.; Malamud, B.D.; Witt, A.; Guzzetti, F. Landslide shape, ellipticity and length-to-width ratios. *Earth Surf. Process. Landf.* **2018**, *43*, 3164–3189. [CrossRef]
61. Malott, N.O.; Sens, A.M.; Wilsey, P.A. Topology Preserving Data Reduction for Computing Persistent Homology. In Proceedings of the 2020 IEEE International Conference on Big Data (Big Data), Atlanta, GA, USA, 10–13 December 2020; IEEE: New York, NY, USA, 2020; pp. 2681–2690.

Disclaimer/Publisher's Note: The statements, opinions and data contained in all publications are solely those of the individual author(s) and contributor(s) and not of MDPI and/or the editor(s). MDPI and/or the editor(s) disclaim responsibility for any injury to people or property resulting from any ideas, methods, instructions or products referred to in the content.